JOURNAL OF PETROLOGY | VOLUME 48 | NUMBER 8 | PAGES 1471–1494 | 2007 | doi:10.1093/petrology/egm026

Variations in Melt Productivity and Melting Conditions along SWIR (70°E–49°E): Evidence from Olivine-hosted and Plagioclase-hosted Melt Inclusions

L. FONT[1]*, B. J. MURTON[1], S. ROBERTS[1] AND A. G. TINDLE[2]

[1]NATIONAL OCEANOGRAPHY CENTRE, UNIVERSITY OF SOUTHAMPTON, EUROPEAN WAY, SOUTHAMPTON SO14 3ZH, UK

[2]DEPARTMENT OF EARTH SCIENCES, THE OPEN UNIVERSITY, WALTON HALL, MILTON KEYNES MK7 6AA, UK

RECEIVED FEBRUARY 25, 2005; ACCEPTED APRIL 25, 2007
ADVANCE ACCESS PUBLICATION MAY 28, 2007

Melt inclusion and host glass compositions from the eastern end of the Southwest Indian Ridge show a progressive depletion in light rare earth elements (LREE), Na_8 and $(La/Sm)_n$, but an increase in Fe_8, from the NE (64°E) towards the SW (49°E). These changes indicate an increase in the degree of mantle melting towards the SW and correlate with a shallowing of the ridge axial depth and increase in crustal thickness. In addition, LREE enrichment in both melt inclusions and host glasses from the NE end of the ridge are compatible with re-fertilization of a depleted mantle source. The large compositional variations (e.g. P_2O_5 and K_2O) of the melt inclusions from the NE end of the ridge (64°E), coupled with low Fe_8 values, suggest that melts from the NE correspond to a variety of different batches of melts generated at shallow levels in the mantle melting column. In contrast, the progressively more depleted compositions and higher Fe_8 values of the olivine- and plagioclase-hosted melt inclusions at the SW end of the studied region (49°E), suggest that these melt inclusions represent batches of melt generated by higher degrees of melting at greater mean depths in the mantle melting column. Systematic differences in Fe_8 values between the plagioclase- and the olivine-hosted melt inclusions in the SW end (49°E) of the studied ridge area, suggest that the plagioclase-hosted melt inclusions represent final batches of melt generated at the top of the mantle melting column, whereas the olivine-hosted melt inclusions correspond to melts generated from less depleted, more fertile mantle at greater depths.

KEY WORDS: *basalt; melt inclusions; olivine; plagioclase; Southwest Indian Ridge*

INTRODUCTION

Melt inclusions are small aliquots of melt trapped in crystals. It is widely considered that melt inclusions preserve the compositional characteristics of early melts before they have mixed and fractionated in magma chambers. Studies of melt inclusions in mid-ocean ridge basalt (MORB) suggest that there is an extensive compositional range of mantle-derived melts under mid-ocean ridges (Sinton & Detrick, 1993; Sobolev & Shimizu, 1993, 1994; Sours-Page *et al.*, 1999, 2002). These studies have shown that melt inclusion compositions vary with spreading rate, crustal thickness and deduced mantle temperature. Under slow-spreading ridges, where the degrees of mantle melting are lower (Reid & Jackson, 1981; McKenzie, 1985; Bown & White, 1994), the magma supply is episodic (Murton & Parson, 1993; Robinson, 1998), and steady-state magma chambers are rare (e.g. Fowler, 1976, 1978; Purdy & Detrick, 1986). Thus, the melts generated have less opportunity to mix, and any original diversity in melt composition is likely to be preserved. In contrast, under fast-spreading ridges, where the melt supply rate is higher, magma accumulates in more permanent, open-system magma chambers. Subsequent mixing results in a less diverse array of melt compositions preserved in melt inclusions (Sours-Page *et al.*, 2002).

In this study, we use melt inclusions hosted in olivine and plagioclase phenocrysts from basalts erupted along a section (69°E–49°E) of the Southwest Indian Ridge

*Corresponding author. Present address: Department of Earth Sciences, Science Laboratories, University of Durham, Durham DH1 3LE, UK. Telephone: +44 (0) 1913342329. Fax: +44 (0) 3342301. E-mail: laura.font@durham.ac.uk

© The Author 2007. Published by Oxford University Press. All rights reserved. For Permissions, please e-mail: journals.permissions@oxfordjournals.org

Downloaded from petrology.oxfordjournals.org by guest on May 18, 2011

(SWIR) in the Indian Ocean (Fig. 1), to test if the diversity of melts generated beneath the mid-ocean ridge varies with inferred changes in the melt flux. The depth of this section of the SWIR shallows from the NE to the SW and correlates with a change from tectonically dominated spreading (NE) to magmatically dominated spreading (SW). The depth also varies with inferred melt flux (Mendel *et al.*, 1997).

Geochemical studies of lavas along the Southwest Indian Ridge show that they are chemically and isotopically different from Atlantic and Pacific MORB (Frey *et al.*, 1980; Le Roex *et al.*, 1983; Price *et al.*, 1986; Mahoney *et al.*, 1989; Natland, 1991; Meyzen *et al.*, 2003). Along its length from 49°E towards the Rodrigues Triple Junction (RTJ) (70°E), the SWIR contains increasingly Na-rich basalts, some of which are the most Na-rich known from the global mid-ocean ridge system (Price *et al.*, 1986; Natland, 1991; Meyzen *et al.*, 2003). The most eastern samples also have high Fe_8 and $(La/Sm)_n$ values. These geochemical features are consistent with lower melt fractions towards the SE,

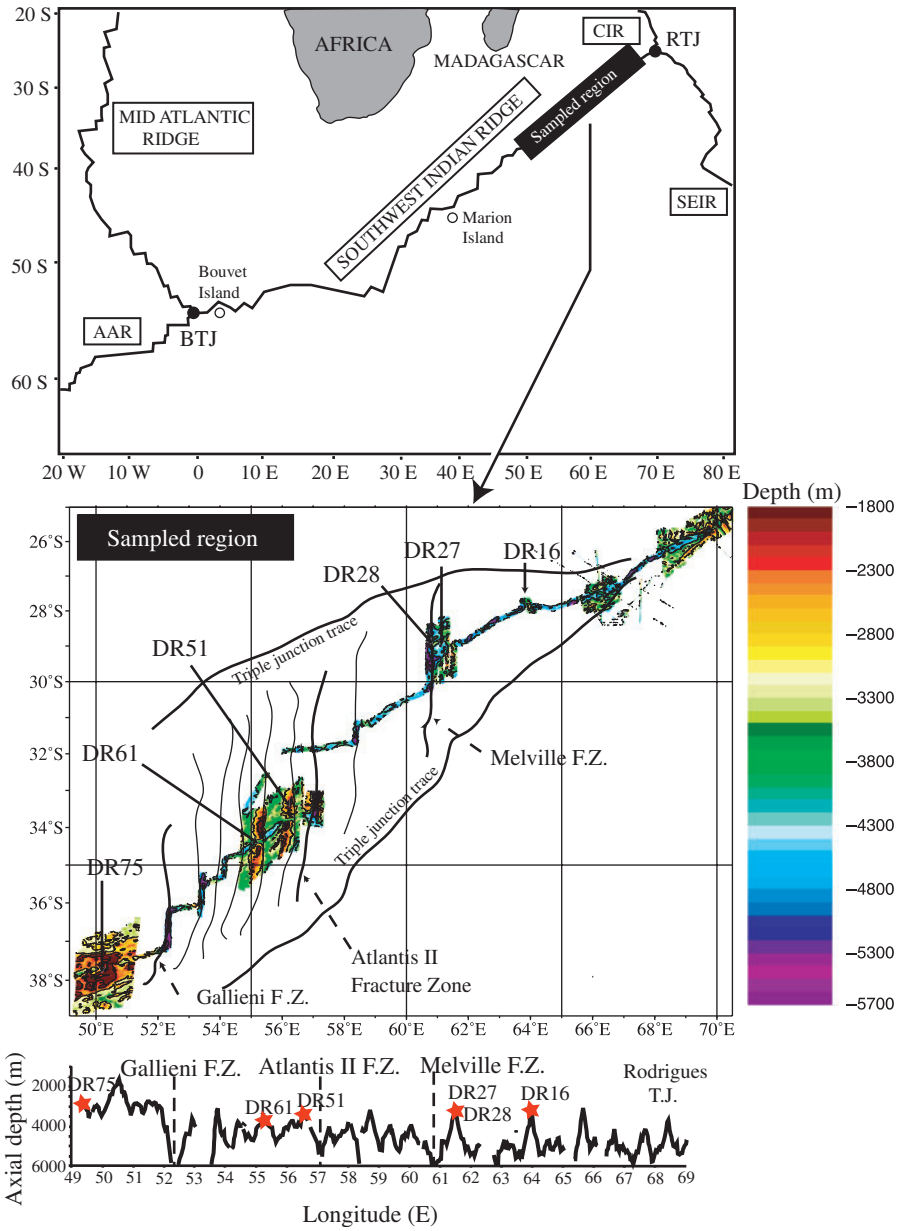

Fig. 1. Location and bathymetry map of the Southwest Indian Ridge between 70°E and 49°E. The profile of the axial depth of the ridge shows the ridge becomes shallower towards the SW emphasized by the arrow. The samples used for this study are marked by stars along the bathymetric profile. RTJ, Rodrigues Triple Junction; SEIR, Southeast Indian Ridge; CIR, Central Indian Ridge; BTJ, Bouvet Triple Junction; AAR, Australian–Antarctic Ridge.

Downloaded from petrology.oxfordjournals.org by guest on May 18, 2011

although Meyzen *et al.* (2003) also identified a component of mantle metasomatism affecting the source of samples east of 61°E.

Although trapped melts, melt inclusions rarely represent the unmodified composition of their host magma. Complications arise from crystallization of the host mineral on inclusion walls, and growth of daughter crystals within inclusions (Roedder, 1984). In the majority of melt inclusion studies, homogenization experiments are carried out to restore the composition of the melt inclusions to that at the moment of entrapment. However, a number of problems are associated with such homogenization experiments. Re-equilibration between melt inclusions and their hosts may occur as a result of slow heating, whereas rapid heating may provide an erroneous temperature of entrapment (Sours-Page *et al.*, 1999; Danyushevsky *et al.*, 2002). Some of these problems can be better controlled if the homogenization experiments are performed under visual control (Danyushevsky *et al.*, 2002). An alternative method of reconstructing the composition of the melt inclusions at the moment of entrapment is to use numerical models, based on the composition of the residual melt in the inclusion, the equilibrium composition of the mineral host and the amount of post-entrapment crystallization (Danyushevsky *et al.*, 2000; Gaetani & Watson, 2002). However, these models can only be applied if re-equilibration between the host and the melt inclusions did not occur during natural cooling and the melt inclusions remain glassy after eruption.

In this study we use numerically reconstructed melt inclusion compositions to investigate melt diversity and mantle processes at the SWIR. The olivine-hosted and plagioclase-hosted melt inclusions used for this study are all naturally glassy. Some, however, have host overgrowth on their walls. These overgrowths are not visible through the optical microscope, but their presence has been detected from the melt inclusion compositions. Inverse modelling is used to calculate the original composition of the melt inclusions at their moment of entrapment.

TECTONIC SETTING AND SAMPLING

The SWIR extends from the Bouvet Triple Junction (BTJ) (54°50′S, 00°40′W) in the South Atlantic Ocean to the Rodrigues Triple Junction (RTJ) (25°30′S, 70°00′E) in the Indian Ocean (Fig. 1). The SWIR is classified as an ultraslow-spreading centre (Dick *et al.*, 2003). Its present-day full spreading rate varies along the ridge from ~16–18 mm/year in the SW to ~12–13 mm/year in the NE (Chu & Gordon, 1999). The NE end of the ridge propagates towards the RTJ and is offset by three major fracture zones oriented north–south (Scalter *et al.*, 1981; de Ribet *et al.*, 1988): the Gallieni Fracture Zone (52·5°E), the Atlantis II Fracture Zone (57°E) and the Melville Fracture Zone (61°E) (Fig. 1). These fracture zones divide the SWIR into three segments, which are characterized from SW to NE by a progressive decrease in the number of axial volcanoes and an increase of the mean axial depth of the ridge (Mendel *et al.*, 1997; Cannat *et al.*, 1999). This broad bathymetric variation suggests thinner crust and/or denser mantle towards the RTJ (Cannat *et al.*, 1999; Sauter *et al.*, 2001). Seismic studies between 61°E and 63°E along the SWIR (Muller *et al.*, 1999, 2000) also suggest the presence of anomalously thin crust, about 4–5 km thick, and Mendel *et al.* (1997) and Cannat *et al.* (1999) suggested that these changes are consequences of a reduced melt supply in the NE part of the SWIR, possibly resulting from lower mantle temperatures compared with the SW part. Minshull & White (1996) and Robinson *et al.* (2001) have further suggested that the lower mantle temperature under the NE end of the SWIR is the result of conductive cooling of the asthenospheric mantle owing to slow upwelling.

The samples investigated for this study (DR16, DR27, DR28, DR51, DR61 and DR75) (Fig. 1) were dredged along the axis of the SWIR [during cruise EDUL Echantillonage d'une Dorsal UltraLente in 1997] (Fig. 1). They are selected from the three main ridge segments delimited by the Melville, Atlantis II and Gallieni fracture zones.

PETROGRAPHY AND MINERAL CHEMISTRY

The samples investigated are fragments of basaltic pillow lavas and sheet flows. They are porphyritic with plagioclase phenocrysts and olivine microphenocrysts in a glassy to cryptocrystalline matrix. Plagioclase is the dominant phenocryst phase. The matrix has a variolitic texture, varying from glassy quenched rims (1–10 mm thick) to more devitrified textures towards the interior of the samples. The matrix from the sample interior contains microcrystalline plagioclase, olivine and spinel with interstitial glass. Plagioclase and olivine crystals located in the rapidly quenched glassy pillow rims were selected for this study, as they are more likely to contain naturally occurring glassy melt inclusions with minimal post-entrapment modification. A total of 140 melt inclusions were analysed, of which 129 are plagioclase-hosted and 11 are olivine-hosted.

Olivine

Olivine occurs both as single euhedral to subhedral phenocrysts ranging in size from 1 mm to 100 μm, and in

Downloaded from petrology.oxfordjournals.org by guest on May 18, 2011

glomero-porphyritic aggregates along with plagioclase. Some of the olivines have partially resorbed rims whereas others contain spinel microlites and rare, glassy melt inclusions (Fig. 2a). Olivine compositions range from Fo_{81} (DR75) to Fo_{87} (DR28) (Table 1). The melt inclusions range from 5 to 80 μm in diameter, are rounded, and contain contraction bubbles.

Plagioclase

Plagioclase phenocrysts range in morphology from euhedral to subhedral shapes, and are between 2 and 20 mm in size. Many crystals have resorbed rims and some exhibit sieve textures. They occur as both single crystals and in glomero-porphyritic aggregates with olivine, and commonly contain olivine and spinel microlites, as well as abundant melt inclusions (Fig. 2b). The plagioclase crystals show normal, reverse and oscillatory zoning ranging from An_{89} (DR75) to An_{62} (DR28) (Table 1). The different zoning types occur in well-defined geographical regions along the SWIR: reverse zoning (i.e. more calcic rims) is typical to the NE of the Melville Fracture Zone (61°E); normal zoning to the SW of the Gallieni Fracture Zone (52°E); and oscillatory zoning mostly in the region between (Mével *et al.*, 2002). The average anorthite content, which is variable for different crystals in the same sample, also varies with position along the SWIR, becoming progressively more anorthitic (more calcic) towards the SW (Table 1).

Primary, rounded, melt inclusions are abundant in nearly all plagioclase phenocrysts, (Fig. 2b). They range from 5 to 100 μm in diameter, are randomly arranged within the centre of the crystal, but commonly aligned parallel to zoning or parallel to twin planes, and usually contain contraction bubbles.

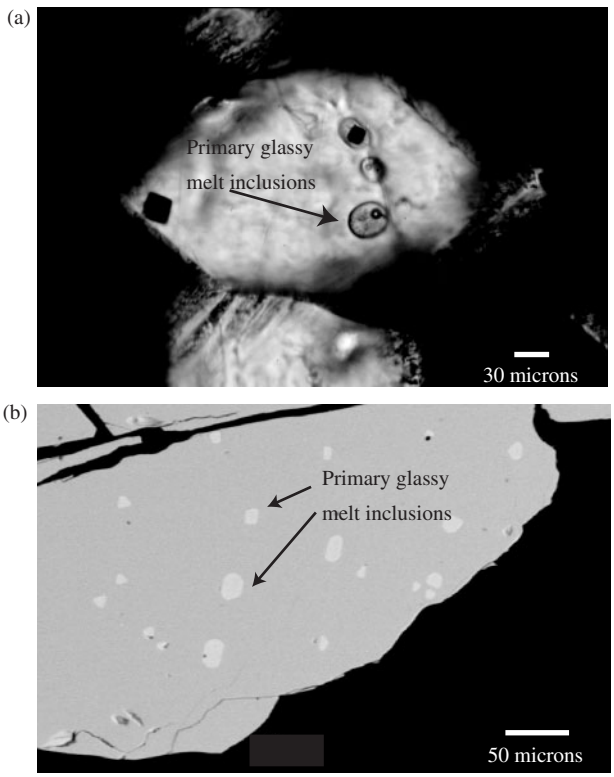

Fig. 2. (a) Glassy olivine-hosted melt inclusions from sample DR28. (b) Backscattered electron image of plagioclase-hosted melt inclusions from sample DR75. Both images illustrate melt inclusions typical of those analysed in this study. The mean size of the inclusions is 30 μm.

ANALYTICAL TECHNIQUES

The pillow rim glasses, the naturally glassy melt inclusions, and the host olivine and plagioclase phenocrysts were analysed for major elements using a Cameca SX100 electron microprobe at the Department of Earth Sciences, The Open University, UK. Pillow rim glasses and host crystals were analysed using an electron beam defocused to 20 μm to maximize the excitation volume while minimizing volatile loss, with an accelerating voltage of 15 kV and a current of 20 nA and an acquisition time of 10 s for each element. Calibration was made against internal standards and the drift was monitored using a naturally occurring kaersutite amphibole. The melt inclusions were analysed using an electron beam of 10 μm diameter because of the small size of the melt inclusions ($\sim$30 μm). Using such a small electron beam increases the volatile loss during analysis; however, volatile loss was considered negligible when the totals of the analyses were between 98·5% and 100%. The acquisition time for each element was 10 s.

The trace element and rare earth element (REE) compositions of pillow rim glasses, glassy melt inclusions and host phenocrysts were determined by ion microprobe analyses, using a Cameca ims-4f at the Department of Geology and Geophysics, University of Edinburgh, UK. The analyses were conducted using a primary beam of negatively charged oxygen ions with a current of 5 nA and net energy of 15 keV. The beam was focused to a spot 20 μm in diameter, which limited the analyses to only the larger melt inclusions (>35 μm). The secondary ions were measured using an energy filtering technique to suppress molecular ion interferences. Only ions of energy 55–75 eV were measured and detected using an electron multiplier. International standard glass BCR (Basalt, Columbia River) was used for the calibration of the matrix glasses, olivine and melt inclusion concentrations, and the SHF (Sapphire Hill Anorthoclase) plagioclase standard (Irving & Frey, 1984) was used for the calibration of plagioclase analyses. Reproducibility on the values of the BCR standard was better than 10%.

Downloaded from petrology.oxfordjournals.org by guest on May 18, 2011

Table 1: Olivine (Ol) and plagioclase (Pl) host phenocrysts compositions

Sample:	DR16	DR16	DR27	DR27	DR28	DR28	DR51	DR51
Phenocrysts:	Pl 1 core	Pl 1 rim	Pl 4 core	Pl 4 rim	Pl 4 core	Pl 4 rim	Pl 1 core	Pl 1 rim
SiO_2	50·77	51·08	52·67	51·47	51·53	50·62	48·52	48·73
TiO_2	0·03	0·04	0·03	0·03	0·06	0·04	0·03	0·02
Al_2O_3	30·87	30·57	29·7	30·47	30·07	31·13	32·31	32·43
FeO	0·28	0·3	0·31	0·24	0·26	0·33	0·43	0·34
MnO	0	0·01	0·02	0	0·01	0	0	0·01
MgO	0·18	0·2	0·19	0·19	0·2	0·13	0·2	0·2
CaO	14·27	14·25	13·29	14·29	14·1	15·26	16·55	16·4
Na_2O	3·47	3·54	4·18	3·71	3·85	3·13	2·34	2·38
K_2O	0·02	0·03	0·03	0·02	0·03	0·01	0·02	0·01
P_2O_5	0·01	0·02	0·01	0·01	0·08	0·06	0·03	0·02
Cr_2O_3	0·04	0	0	0	0	0	0·01	0
Total	99·94	100·04	100·43	100·43	100·19	100·71	100·44	100·54
Ba	4·9	n.a.	3·3	n.a.	2·5	n.a.	1·4	n.a.
Nb	n.a.	n.a.	n.a.	n.a.	n.a.	n.a.	n.a.	n.a.
La	0·4	n.a.	0·3	n.a.	0·3	n.a.	0·1	n.a.
Ce	0·7	n.a.	0·5	n.a.	0·6	n.a.	0·3	n.a.
Pr	n.a.	n.a.	n.a.	n.a.	n.a.	n.a.	n.a.	n.a.
Sr	373	n.a.	344	n.a.	262	n.a.	167	n.a.
Nd	n.a.	n.a.	n.a.	n.a.	n.a.	n.a.	n.a.	n.a.
Hf	n.a.	n.a.	n.a.	n.a.	n.a.	n.a.	n.a.	n.a.
Zr	n.a.	n.a.	n.a.	n.a.	n.a.	n.a.	n.a.	n.a.
Sm	n.a.	n.a.	n.a.	n.a.	n.a.	n.a.	n.a.	n.a.
Eu	0·2	n.a.	0·2	n.a.	0·2	n.a.	0·1	n.a.
Gd	n.a.	n.a.	n.a.	n.a.	n.a.	n.a.	n.a.	n.a.
Tb	n.a.	n.a.	n.a.	n.a.	n.a.	n.a.	n.a.	n.a.
Dy	n.a.	n.a.	n.a.	n.a.	n.a.	n.a.	n.a.	n.a.
Y	n.a.	n.a.	n.a.	n.a.	n.a.	n.a.	n.a.	n.a.
Ho	n.a.	n.a.	n.a.	n.a.	n.a.	n.a.	n.a.	n.a.
Er	n.a.	n.a.	n.a.	n.a.	n.a.	n.a.	n.a.	n.a.
Yb	n.a.	n.a.	n.a.	n.a.	n.a.	n.a.	n.a.	n.a.
Host:	An_{69}	An_{70}	An_{64}	An_{68}	An_{62}	An_{69}	An_{81}	An_{81}

(continued)

Downloaded from petrology.oxfordjournals.org by guest on May 18, 2011

Table 1: Continued

Sample:	DR16	DR16	DR27	DR27	DR28	DR28	DR51	DR51
Phenocrysts:	Pl 1 core	Pl 1 rim	Pl 4 core	Pl 4 rim	Pl 4 core	Pl 4 rim	Pl 1 core	Pl 1 rim
SiO_2	48·98	47·62	46·43	45·67	40·74	40·51	39·28	38·99
TiO_2	0·04	0·03	0·03	0·02	0	0	0·03	0·04
Al_2O_3	31·84	33·01	33·91	34·01	0·04	0·04	0·02	0·04
FeO	0·35	0·35	0·27	0·4	13·02	12·81	16·76	17·69
MnO	0·01	0	0	0	0·21	0·21	0·23	0·3
MgO	0·2	0·14	0·27	0·17	45·98	46·64	43·43	42·65
CaO	15·67	16·68	17·78	18·34	0·3	0·28	0·3	0·4
Na_2O	2·71	2·08	1·34	1·26	0·01	0·04	0·02	0·01
K_2O	0·03	0·03	0	0	0	0	0·01	0
P_2O_5	0·01	0·01	0·02	0	0·04	0	0·03	0·1
Cr_2O_3	0·01	0·01	0	0·03	0·04	0·06	0·02	0·05
Total	99·85	99·96	100·05	99·9	100·59	100·59	100·13	100·27
Ba	2·1	n.a.	0·8	n.a.	n.a.	0·1	0·46	n.a.
Nb	n.a.	n.a.	n.a.	n.a.	n.a.	0·003	0·004	n.a.
La	0·2	n.a.	0·07	n.a.	n.a.	0·013	0·29	n.a.
Ce	0·4	n.a.	0·1	n.a.	n.a.	0·02	0·04	n.a.
Pr	n.a.	n.a.	n.a.	n.a.	n.a.	0·03	0·014	n.a.
Sr	176	n.a.	82	n.a.	n.a.	0·19	0·34	n.a.
Nd	n.a.	n.a.	n.a.	n.a.	n.a.	0·013	0·15	n.a.
Hf	n.a.	n.a.	n.a.	n.a.	n.a.	0·006	0·02	n.a.
Zr	n.a.	n.a.	n.a.	n.a.	n.a.	0·12	0·2	n.a.
Sm	n.a.	n.a.	n.a.	n.a.	n.a.	0·005	0·05	n.a.
Eu	0·2	n.a.	0·07	n.a.	n.a.	0·003	0·03	n.a.
Gd	n.a.	n.a.	n.a.	n.a.	n.a.	0·008	0·02	n.a.
Tb	n.a.	n.a.	n.a.	n.a.	n.a.	0·002	0·01	n.a.
Dy	n.a.	n.a.	n.a.	n.a.	n.a.	0·007	n.a.	n.a.
Y	n.a.	n.a.	n.a.	n.a.	n.a.	0·15	0·24	n.a.
Ho	n.a.	n.a.	n.a.	n.a.	n.a.	0·005	n.a.	n.a.
Er	n.a.	n.a.	n.a.	n.a.	n.a.	0·042	0·05	n.a.
Yb	n.a.	n.a.	n.a.	n.a.	n.a.	0·09	0·2	n.a.
Host	An_{76}	An_{82}	An_{88}	An_{89}	Fo_{86}	Fo_{87}	Fo_{82}	Fo_{81}

Major element compositions are in wt % and trace element concentrations are in μg/g. n.a., not analysed.

PILLOW RIM GLASS AND MELT INCLUSION COMPOSITIONS

Major elements

The pillow rim glasses show a general westward increase in FeO, TiO_2 and CaO concentration and a decrease in Al_2O_3, Na_2O and K_2O, between 64°E and 49°E along the SWIR (Fig. 3; Table 2). At a local scale, however, at specific locations along the ridge, the glasses show large variations in TiO_2, P_2O_5 and K_2O (e.g. at 59°E). In the studied samples, pillow rim glasses at 55°E (DR61) have the highest concentration in TiO_2 and P_2O_5 but the lowest in MgO compared with the host glasses from the rest of the studied samples. The observed major element trends can be reproduced by calculated fractional crystallization liquid lines of descent (LLD). The fractionation trends and the parental magmas (Table 3) were determined by reverse fractional crystallization calculations (using the program 'Petrolog v.2', Danyushevsky, 2001), involving the addition of olivine, plagioclase and clinopyroxene to the known composition of the pillow rim glasses, such that the final liquids are in equilibrium with mantle olivine (Fo_{90}). Plagioclase fractionation was initiated when the liquids reached an

Downloaded from petrology.oxfordjournals.org by guest on May 18, 2011

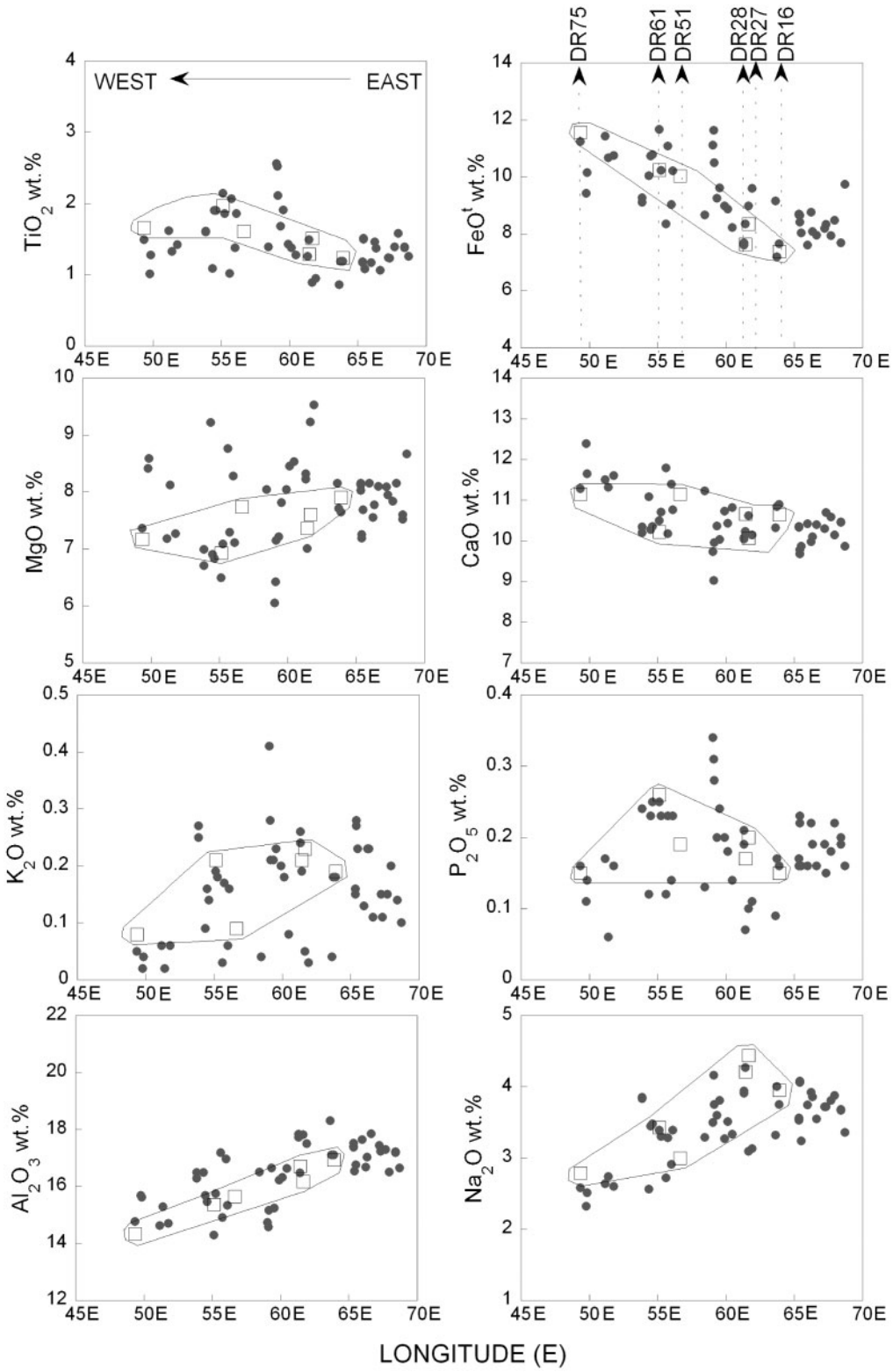

Fig. 3. Major element compositions vs longitude (°E) of Southwest Indian Ridge glasses (Meyzen *et al.*, 2003) (●) compared with host glasses from this study (□).

Downloaded from petrology.oxfordjournals.org by guest on May 18, 2011

Table 2: Host glass composition of samples from the Southwest Indian Ridge between 64° E and 49° E

Sample:	DR16	DR27	DR28	DR51*	DR61	DR75
Long. (E):	63·91	61·65	61·44	56·64	55·13	49·34
SiO_2	51·44	50·15	51·48	49·04	50·11	49·94
TiO_2	1·24	1·51	1·29	1·61	1·97	1·66
Al_2O_3	16·93	16·17	16·71	15·65	15·36	14·34
FeO	7·38	8·34	7·64	11·16	10·25	11·57
MnO	0·15	0·16	0·15	0·17	0·19	0·21
MgO	7·91	7·61	7·36	7·74	6·93	7·17
CaO	10·64	10·06	10·66	11·15	10·22	11·15
Na_2O	3·95	4·44	4·21	3	3·43	2·79
K_2O	0·19	0·23	0·21	0·09	0·21	0·08
P_2O_5	0·15	0·2	0·17	0·19	0·26	0·15
Cr_2O_3	0·05	0·04	0·04	n.a	0·04	0·05
Total	100·03	98·91	99·92	99·8	98·97	99·11
Ba	17·8	12·2	15·8	8·1	20·3	8·5
Nb	3·7	3·2	4·2	1·9	4·6	1·8
La	5·4	5·7	6·3	3·7	7·9	2·8
Ce	15·7	16·4	18	12·9	24·5	9·7
Pr	2·4	2·6	2·6	2·3	4·04	1·8
Sr	207	200	198	107	151	78·9
Nd	11·4	11·7	13·2	12·6	20·4	10·6
Hf	2·5	2·1	2·7	2·6	4·9	2·7
Zr	113	122	134	118	199	100
Sm	3·3	3·6	4·1	4·6	6·6	3·9
Eu	0·9	0·8	0·9	1·1	1·5	1·1
Gd	3·6	3·4	4·07	4·8	6·6	4·9
Tb	0·6	0·6	0·7	0·9	1·3	0·9
Dy	4·7	3·9	4·7	6·1	8·3	6·7
Y	28·4	28·5	32·6	42·5	54·7	48·3
Ho	0·9	0·8	1	1·2	1·7	1·5
Er	3·1	2·6	3	4	5·7	4·6
Yb	2·6	2·7	3	3·8	5·3	4·6

*Major elements from Meyzen *et al*. (2003); n.a, not analysed.

MgO content of between 9 and 10 wt %; glasses with MgO <9–10 wt % define an olivine + plagioclase cotectic (Fig. 4).

The olivine-hosted melt inclusions are characterized by low MgO and high Al_2O_3 concentrations compared with the pillow rim glasses. Plagioclase-hosted melt inclusions are generally characterized by large variations in MgO, Al_2O_3, TiO_2 and FeO compared with the host glasses (Fig. 4 and Table 4). The variations in MgO and Al_2O_3 in naturally glassy melt inclusions indicate post-entrapment crystallization of the host crystal on the walls of the inclusion, resulting in compositions that are depleted in elements that are compatible with the host crystal (e.g. MgO for olivine and Al_2O_3 for plagioclase). The composition of the melt inclusion at the moment of entrapment was estimated by calculating the reverse of the host crystallization on the walls of the inclusion until the composition reached the olivine + plagioclase cotectic (Fig. 4 and Table 5). The recalculated melt inclusion compositions plot consistently along the liquid line of descent on the MgO vs Al_2O_3 diagram. However, for other major elements (e.g. TiO_2 and Na_2O) some of the reconstructed melt inclusion compositions plot outside the LLD defined by the glasses. There are melt inclusions that are low in TiO_2 and FeO compared with the host glass, and that remain low after recalculation. They also show

Downloaded from petrology.oxfordjournals.org by guest on May 18, 2011

Table 3: Calculated parental melt composition

	PM-DR16	PM-DR27	PM-DR28	PM-DR51	PM-DR61	PM-DR75
SiO_2	50·63	50·00	50·46	47·25	48·37	49·17
TiO_2	0·98	1·04	0·93	0·80	0·99	0·67
Al_2O_3	18·33	18·51	18·58	19·92	19·65	17·60
FeO*	6·54	6·86	6·46	7·53	7·11	6·43
MnO	0·12	0·12	0·12	0·11	0·12	0·12
MgO	8·78	9·05	8·64	10·37	9·83	9·65
CaO	10·62	10·13	10·59	11·55	10·85	14·44
Na_2O	3·64	3·96	3·76	2·23	2·64	1·84
K_2O	0·15	0·16	0·15	0·05	0·10	0·05
P_2O_5	0·12	0·14	0·12	0·10	0·13	0·00
Cr_2O_3	0·04	0·03	0·03	0·00	0·03	0·00
H2O	0·06	0·00	0·16	0·09	0·18	0·04
Total	100	100	100	100	100	100
Equilibrium olivine	90·1	90·1	90·1	90·1	90·2	90·8

*Total iron given as FeO.
The major element compositions are in wt %.

anomalous concentrations in other major elements (e.g. Na_2O) and plot outside the general MORB field (Fig. 4). These extraordinary compositions have been discarded from subsequent interpretations as we believe they do not represent the composition of any possible mantle-derived melt and are products of additional post-entrapment processes. Figure 4 illustrates the compositional differences before and after correction for the olivine- and plagioclase-hosted melt inclusions from sample DR28.

The non-discarded recalculated olivine- and plagioclase-hosted melt inclusion compositions (Table 5) have been plotted against longitude (Fig. 5), where they follow the general trend displayed by the host glasses. The melt inclusions show large compositional ranges in K_2O and P_2O_5, particularly those in samples collected from locations between 64°E and 61°E (Fig. 5). Some of the recalculated compositions of plagioclase-hosted melt inclusions from samples at 61°E (DR27 and DR28) and 49°E (DR75) have lower concentrations of FeO and TiO_2 compared with the olivine-hosted melt inclusions and host glass compositions (Fig. 5).

Trace elements

The melt inclusions show a general westward decrease in enrichment of light REE (LREE) relative to heavy REE (HREE) (Fig. 6). Those from samples collected between 64°E–61°E (DR16–DR28) and 55°E (DR51) are more enriched in LREE compared with the melt inclusions at 55°E (DR51) and at 49°E (DR75).

INTERPRETATION

Melt inclusion compositional variations

The recalculated major element concentrations of the olivine-hosted and plagioclase-hosted melt inclusions display a similar trend to that shown by the SWIR glasses (Fig. 5). Both matrix glasses and melt inclusions decrease in Al_2O_3, Na_2O and K_2O concentration, but increase in FeO and CaO, from the NE (64°E) to the SW (49°E) along the SWIR. This suggests an increase in the degree of fractional crystallization of the melt towards the SW. Some recalculated plagioclase-hosted melt inclusion compositions, particularly those from sample DR75 at 49°E, are low in FeO and TiO_2 compared with the matrix glass and olivine-hosted melt inclusions. Danyushevsky *et al.* (2002) described the low TiO_2 and FeO contents of such melt inclusions as a common feature in MORB, and suggested that they are caused by pre-eruption re-equilibration by diffusion of Fe and Ti out of the melt inclusions into the host plagioclase, and diffusion of Si from the host into the melt inclusions. In contrast, Kohut & Nielsen (2004) demonstrated that depletions in Fe–Ti and the large K_2O variability observed in natural MORB melt inclusions hosted in An-rich plagioclase phenocrysts are not the product of post-entrapment processes. Their experimental results imply that the compositional variability observed in the melt inclusions reflects melt trapped at earlier stages. Thus, the compositional diversity in the melt inclusions represents trapped host melt that changed in composition with time and increasing

Downloaded from petrology.oxfordjournals.org by guest on May 18, 2011

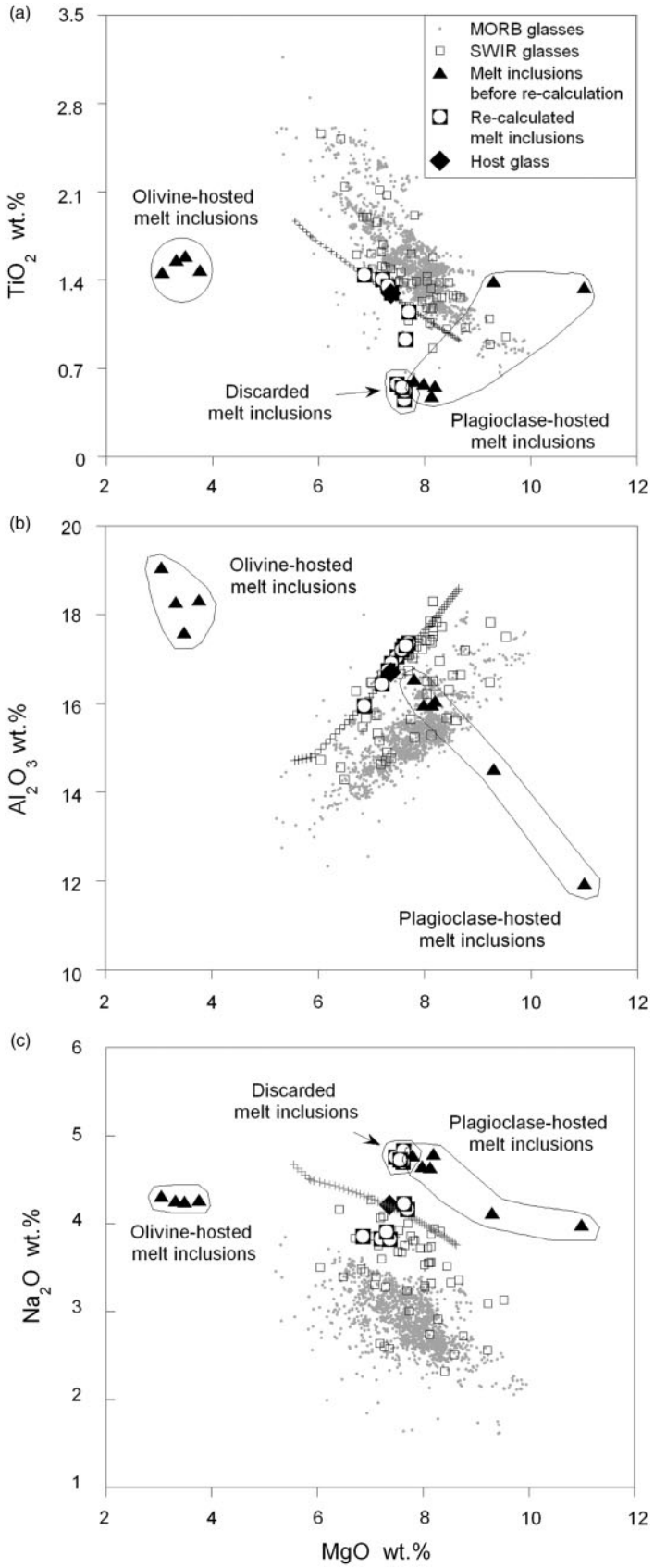

Fig. 4. TiO_2 (a), Al_2O_3 (b) and Na_2O (c) vs MgO wt % variation diagrams of melt inclusion compositions before recalculation (▲), after recalculation (white circles in a square frame) and host glass (◆). A small number of recalculated melt inclusion compositions still have anomalous compositions. These are discarded from subsequent consideration. Also shown are global MORB glass compositions (•) (Smithsonian Institution Catalogue, available at www.minerals.si.edu/research/glass/), Southwest Indian Ridge glass compositions (Meyzen *et al.*, 2003) (□) and liquid line of descent (calculated using the program 'Petrolog v.2, Danyushevsky, 2001) (+).

Downloaded from petrology.oxfordjournals.org by guest on May 18, 2011

Table 4: Representative uncorrected olivine- and plagioclase-hosted melt inclusions compositions from samples of the Southwest Indian Ridge (64°E–49°E)

Sample:	DR16	DR16*	DR27	DR27	DR27*	DR28	DR28	DR28*
MI:	AS-19	AT-20	CS	AL-12	AK-9	34	DH-84	3
Host:	Pl 1	Pl 1	Pl 4	Ol 5	Pl 4	Pl 4	Ol 4	Pl 4
SiO_2	51·89	54·31	53·05	52·84	53·4	50·34	52·63	52·28
TiO_2	1·38	0·64	0·95	1·66	0·72	1·51	1·56	0·56
Al_2O_3	14·06	14·43	16·35	18·44	15·86	13·99	18·29	16·06
FeO	9·03	8·23	7·35	7·27	8·02	8·84	7·23	7·21
MnO	0·17	0·16	0·13	0·14	0·14	0·15	0·13	0·16
MgO	9·66	8·55	8·45	3·69	8·9	10·01	3·32	8·19
CaO	9·53	8·89	9·17	11·40	8·14	10·32	12·08	9·22
Na_2O	4·07	4·43	4·54	4·51	4·86	3·71	4·26	4·79
K_2O	0·37	0·42	0·22	0·22	0·34	0·20	0·23	0·35
P_2O_5	0·17	0·03	0·10	0·21	0·01	0·16	0·25	0·02
Cr_2O_3	0·04	0·02	0·03	0·00	0·07	0·08	0·06	0·06
Total	100·4	100·1	100·3	100·4	100·5	99·3	100·0	98·9
Ba	24·23	27·86	16·64	18·46	12·60	n.d.	16·55	10·66
Nb	4·07	0·13	2·59	4·76	0·17	n.d.	4·34	0·19
La	6·15	3·76	4·26	7·68	4·10	n.d.	6·33	2·88
Ce	17·53	9·91	12·87	23·80	11·95	n.d.	17·23	8·26
Pr	2·44	1·42	1·93	3·56	1·99	n.d.	2·67	1·26
Sr	121	150	169	241	143	n.d.	195	145
Nd	11·10	5·99	8·78	16·85	8·91	n.d.	11·96	6·19
Hf	1·77	–	1·54	2·93	0·30	n.d.	3·12	0·08
Zr	56·11	2·72	108	169	4·98	n.d.	103	15·03
Sm	4·15	1·97	2·59	5·56	2·36	n.d.	3·51	1·75
Eu	0·95	0·77	0·86	1·29	0·92	n.d.	0·89	0·67
Gd	3·97	1·38	2·88	5·36	2·59	n.d.	4·20	1·58
Tb	0·71	0·22	0·47	1·03	0·35	n.d.	0·74	0·25
Dy	4·77	1·41	3·41	6·27	2·70	n.d.	4·61	1·71
Y	29·54	7·77	20·37	40·89	19·45	n.d.	34·25	11·24
Ho	0·85	0·19	0·66	1·33	0·56	n.d.	1·04	0·28
Er	2·86	0·68	2·08	4·12	1·49	n.d.	3·01	1·39
Yb	3·01	0·77	1·54	4·01	1·92	n.d.	3·06	0·88
Host core	An_{69}	An_{69}	An_{64}	Fo_{86}	An_{64}	An_{62}	Fo_{87}	An_{62}
Host rim	An_{70}	An_{70}	An_{68}		An_{68}	An_{69}		An_{69}

(continued)

Downloaded from petrology.oxfordjournals.org by guest on May 18, 2011

Table 4: Continued

Sample:	DR51	DR51	DR61	DR61	DR61	DR75	DR75	DR75*
MI:	EA	EE	AC-107	AL-114	150	CH-101	HH-100	EP-29
Host:	Pl 1	Pl 1	Pl 4	Pl 4	Ol 1	Pl 3	Ol 2	Pl 2
SiO_2	50·49	50·72	50·63	49·56	50·52	50·79	50·50	50·75
TiO_2	1·30	1·22	1·19	1·82	2·22	0·73	1·76	0·42
Al_2O_3	15·00	15·03	14·75	14·46	16·59	13·43	15·25	13·53
FeO	9·55	9·59	9·82	10·24	9·03	8·83	11·29	7·66
MnO	0·18	0·17	0·19	0·17	0·19	0·16	0·20	0·16
MgO	8·43	8·63	8·36	8·58	2·87	10·69	4·79	12·24
CaO	11·32	11·09	10·70	10·88	11·80	12·84	12·13	12·99
Na_2O	3·25	3·10	2·97	3·04	3·70	2·04	2·89	1·97
K_2O	0·10	0·10	0·17	0·16	0·21	0·03	0·07	0·03
P_2O_5	0·13	0·12	0·12	0·21	0·33	0·05	0·14	0·01
Cr_2O_3	0·07	0·06	0·07	0·05	0·05	0·09	0·03	0·10
Total	99·8	99·8	99·0	99·2	97·5	99·7	99·0	99·9
Ba	8·80	8·99	12·95	17·37	17·04	5·17	n.a.	4·38
Nb	1·21	1·81	2·21	3·83	3·83	0·23	n.a.	0·17
La	2·51	2·96	3·57	5·73	6·01	1·25	n.a.	1·13
Ce	8·89	8·57	10·83	18·00	18·40	4·14	n.a.	3·44
Pr	1·43	1·49	1·80	2·97	3·07	0·84	n.a.	0·61
Sr	107	103	144	141	144	65	n.a.	50·35
Nd	9·00	8·32	8·87	15·39	16·31	5·30	n.a.	3·72
Hf	2·49	2·02	2·41	3·64	3·26	0·94	n.a.	0·35
Zr	78	82	80	147	151	22·25	n.a.	17·16
Sm	3·03	2·79	3·40	5·64	5·44	2·35	n.a.	1·43
Eu	1·02	0·85	1·03	1·15	0·98	0·63	n.a.	0·49
Gd	3·88	3·26	3·24	5·75	5·33	2·81	n.a.	1·68
Tb	0·80	0·59	0·61	0·96	1·02	0·53	n.a.	0·28
Dy	4·20	3·73	4·24	6·93	7·19	3·44	n.a.	1·63
Y	29·33	27·53	27·98	44·45	45·77	25·11	n.a.	13·36
Ho	0·86	0·82	0·87	1·37	1·63	0·81	n.a.	0·35
Er	2·78	2·52	2·59	4·25	4·59	2·56	n.a.	1·19
Yb	2·59	2·73	2·30	4·04	4·11	2·32	n.a.	0·93
Host core	An_{81}	An_{81}	An_{76}	An_{76}	Fo_{82}	An_{85}	Fo_{81}	An_{88}
Host rim	An_{81}	An_{81}	An_{82}	An_{82}		An_{83}		An_{89}

*HFSE- and HREE-depleted melt inclusions.
MI, melt inclusion; n.a., not analysed. The full dataset is available in Electronic Appendix 1 at http://www.petrology.oxfordjournals.org.

crystallization, and that the final host lava composition is the result of the complete mixing of a number of compositionally diverse magma batches. From this, it follows that the compositional variability of the melt inclusion compositions in this study are likely to represent the original diversity of melts present in the magma storage system. The fact that some melt inclusions plot outside the liquid lines of descent of the host glasses for some major elements, but within the SWIR and the MORB field (Fig. 4c), is evidence for a diversity of parental melts. The accumulation and mixture of all these melts result in the final host lava composition.

Other studies (Nielsen & Sours-Page, 2000; Michael *et al.*, 2002) have shown that plagioclase-hosted melt inclusions can also display depletions in high field strength elements (HFSE) and HREE relative to the host glasses, similar to the depletions observed in the discarded melt inclusions in this study (Table 4 and Supplementary

Downloaded from petrology.oxfordjournals.org by guest on May 18, 2011

Table 5: Corrected olivine and plagioclase hosted melt inclusions compositions from samples of the Southwest Indian Ridge (64°E–49°E)

Sample:	DR16	DR16	DR27	DR27	DR27	DR27	DR27	DR28	DR28	DR28	DR28
MI:	AS-19	BB-28	CS	CW	AD-AH	BG	AL-12	127-130	62	136-138	34
Host:	Pl 1	Pl 1	Pl 4	Pl 4	Pl 1	Pl 4	Ol 5	Pl 4	Pl 4	Pl 4	Pl 4
SiO_2	51·81	52·80	52·82	52·27	51·34	50·61	51·28	51·63	52·17	51·38	50·84
TiO_2	1·11	1·15	0·90	1·05	1·28	1·17	1·49	1·15	0·93	1·17	1·19
Al_2O_3	16·97	16·64	16·96	17·02	17·21	17·58	16·52	17·37	17·31	17·47	17·69
FeO*	7·54	7·28	7·07	7·05	7·53	7·66	8·27	7·28	7·38	7·23	7·19
MnO	0·14	0·15	0·12	0·13	0·14	0·15	0·15	0·12	0·13	0·14	0·12
MgO	7·86	7·54	8·00	8·03	8·14	8·33	7·63	7·70	7·64	7·80	7·91
CaO	9·99	9·92	9·29	9·76	9·99	10·27	10·24	10·23	9·99	10·45	10·96
Na_2O	4·11	4·20	4·51	4·36	3·99	3·92	4·04	4·16	4·23	4·00	3·77
K_2O	0·30	0·27	0·21	0·18	0·16	0·16	0·20	0·24	0·21	0·22	0·16
P_2O_5	0·14	0·05	0·10	0·13	0·18	0·13	0·19	0·13	0·00	0·15	0·13
Cr_2O_3	0·03	0·02	0·03	0·03	0·04	0·04	0·00	0·00	0·01	0·00	0·06
Ba	24·23	n.a.	16·64	n.a.	n.a.	n.a.	18·46	n.a.	n.a.	n.a.	n.a.
Nb	4·07	n.a.	2·59	n.a.	n.a.	n.a.	4·76	n.a.	n.a.	n.a.	n.a.
La	6·15	n.a.	4·26	n.a.	n.a.	n.a.	7·68	n.a.	n.a.	n.a.	n.a.
Ce	17·53	n.a.	12·87	n.a.	n.a.	n.a.	23·80	n.a.	n.a.	n.a.	n.a.
Pr	2·44	n.a.	1·93	n.a.	n.a.	n.a.	3·56	n.a.	n.a.	n.a.	n.a.
Sr	121	n.a.	169	n.a.	n.a.	n.a.	241	n.a.	n.a.	n.a.	n.a.
Nd	11·10	n.a.	8·78	n.a.	n.a.	n.a.	16·85	n.a.	n.a.	n.a.	n.a.
Hf	1·77	n.a.	1·54	n.a.	n.a.	n.a.	2·93	n.a.	n.a.	n.a.	n.a.
Zr	56·11	n.a.	108	n.a.	n.a.	n.a.	169	n.a.	n.a.	n.a.	n.a.
Sm	4·15	n.a.	2·59	n.a.	n.a.	n.a.	5·56	n.a.	n.a.	n.a.	n.a.
Eu	0·95	n.a.	0·86	n.a.	n.a.	n.a.	1·29	n.a.	n.a.	n.a.	n.a.
Gd	3·97	n.a.	2·88	n.a.	n.a.	n.a.	5·36	n.a.	n.a.	n.a.	n.a.
Tb	0·71	n.a.	0·47	n.a.	n.a.	n.a.	1·03	n.a.	n.a.	n.a.	n.a.
Dy	4·77	n.a.	3·41	n.a.	n.a.	n.a.	6·27	n.a.	n.a.	n.a.	n.a.
Y	29·54	n.a.	20·37	n.a.	n.a.	n.a.	40·89	n.a.	n.a.	n.a.	n.a.
Ho	0·85	n.a.	0·66	n.a.	n.a.	n.a.	1·33	n.a.	n.a.	n.a.	n.a.
Er	2·86	n.a.	2·08	n.a.	n.a.	n.a.	4·12	n.a.	n.a.	n.a.	n.a.
Yb	3·01	n.a.	1·54	n.a.	n.a.	n.a.	4·01	n.a.	n.a.	n.a.	n.a.

(continued)

Downloaded from petrology.oxfordjournals.org by guest on May 18, 2011

Table 5: Continued

Sample:	DR28	DR28	DR28	DR28	DR28	DR28	DR28	DR28	DR28	DR28	DR28
MI.:	44	45	85	93	118	197	198	199	201	202	16b
Host:	Pl 4	Pl 4	Pl 4	Pl 4	Pl 4	Pl 4	Pl 4	Pl 4	Pl 4	Pl 4	Pl 4
SiO_2	51·99	52·13	52·54	51·17	51·64	51·94	52·69	52·86	53·00	52·70	51·73
TiO_2	1·18	0·73	0·82	1·24	1·19	1·11	0·79	0·77	0·80	0·77	1·18
Al_2O_3	17·03	17·22	17·08	16·90	17·26	17·13	17·20	17·08	17·17	17·23	17·05
FeO*	7·03	7·23	7·22	7·59	7·37	7·01	7·01	6·93	6·89	7·09	7·35
MnO	0·19	0·13	0·12	0·17	0·15	0·13	0·08	0·16	0·13	0·18	0·13
MgO	7·59	7·77	7·58	7·51	7·69	7·67	7·67	7·67	7·65	7·71	7·63
CaO	10·15	10·43	10·11	10·52	9·75	10·28	9·84	9·52	9·63	9·39	10·29
Na_2O	4·45	4·09	4·30	4·45	4·49	4·28	4·48	4·62	4·40	4·59	4·26
K_2O	0·18	0·20	0·23	0·23	0·26	0·23	0·25	0·27	0·21	0·30	0·23
P_2O_5	0·18	0·02	0·00	0·22	0·17	0·14	0·01	0·04	0·06	0·00	0·15
Cr_2O_3	0·04	0·05	0·00	0·03	0·04	0·08	0·00	0·09	0·08	0·05	0·00
Ba	n.a.	n.a.	n.a.	n.a.	n.a.	n.a.	n.a.	n.a.	n.a.	n.a.	n.a.
Nb	n.a.	n.a.	n.a.	n.a.	n.a.	n.a.	n.a.	n.a.	n.a.	n.a.	n.a.
La	n.a.	n.a.	n.a.	n.a.	n.a.	n.a.	n.a.	n.a.	n.a.	n.a.	n.a.
Ce	n.a.	n.a.	n.a.	n.a.	n.a.	n.a.	n.a.	n.a.	n.a.	n.a.	n.a.
Pr	n.a.	n.a.	n.a.	n.a.	n.a.	n.a.	n.a.	n.a.	n.a.	n.a.	n.a.
Sr	n.a.	n.a.	n.a.	n.a.	n.a.	n.a.	n.a.	n.a.	n.a.	n.a.	n.a.
Nd	n.a.	n.a.	n.a.	n.a.	n.a.	n.a.	n.a.	n.a.	n.a.	n.a.	n.a.
Hf	n.a.	n.a.	n.a.	n.a.	n.a.	n.a.	n.a.	n.a.	n.a.	n.a.	n.a.
Zr	n.a.	n.a.	n.a.	n.a.	n.a.	n.a.	n.a.	n.a.	n.a.	n.a.	n.a.
Sm	n.a.	n.a.	n.a.	n.a.	n.a.	n.a.	n.a.	n.a.	n.a.	n.a.	n.a.
Eu	n.a.	n.a.	n.a.	n.a.	n.a.	n.a.	n.a.	n.a.	n.a.	n.a.	n.a.
Gd	n.a.	n.a.	n.a.	n.a.	n.a.	n.a.	n.a.	n.a.	n.a.	n.a.	n.a.
Tb	n.a.	n.a.	n.a.	n.a.	n.a.	n.a.	n.a.	n.a.	n.a.	n.a.	n.a.
Dy	n.a.	n.a.	n.a.	n.a.	n.a.	n.a.	n.a.	n.a.	n.a.	n.a.	n.a.
Y	n.a.	n.a.	n.a.	n.a.	n.a.	n.a.	n.a.	n.a.	n.a.	n.a.	n.a.
Ho	n.a.	n.a.	n.a.	n.a.	n.a.	n.a.	n.a.	n.a.	n.a.	n.a.	n.a.
Er	n.a.	n.a.	n.a.	n.a.	n.a.	n.a.	n.a.	n.a.	n.a.	n.a.	n.a.
Yb	n.a.	n.a.	n.a.	n.a.	n.a.	n.a.	n.a.	n.a.	n.a.	n.a.	n.a.

(continued)

Downloaded from petrology.oxfordjournals.org by guest on May 18, 2011

Table 5: Continued

Sample:	DR28	DR28	DR28	DR28	DR28	DR28	DR28	DR28	DR28	DR28	DR51
MI:	23b	30b	54b	84b	120b	KA-1	DH-84	DJ-86	DD-80	DL-88	EA
Host:	Pl 4	Pl 4	Pl 4	Pl 4	Pl 4	Ol 4	Ol 4	Ol 4	Ol 4	Ol 4	Pl 1
SiO_2	51·59	52·14	52·16	51·71	52·15	51·45	51·22	51·22	51·45	50·77	50·54
TiO_2	1·15	0·92	1·01	1·09	0·76	1·29	1·40	1·44	1·29	1·35	1·21
Al_2O_3	17·03	17·28	17·13	17·10	17·33	16·90	16·44	15·94	16·90	16·75	16·14
FeO*	7·29	7·46	7·06	7·22	7·18	8·01	8·39	9·00	8·01	8·26	9·04
MnO	0·15	0·13	0·14	0·10	0·17	0·16	0·15	0·18	0·16	0·16	0·17
MgO	7·56	7·66	7·69	7·52	7·71	7·38	7·20	6·86	7·38	7·31	7·86
CaO	10·39	9·97	10·08	10·28	9·98	10·56	10·88	11·05	10·56	11·10	11·50
Na_2O	4·48	4·17	4·36	4·50	4·36	3·82	3·83	3·85	3·82	3·90	3·27
K_2O	0·21	0·26	0·27	0·22	0·28	0·20	0·21	0·19	0·20	0·17	0·09
P_2O_5	0·12	0·02	0·11	0·14	0·06	0·19	0·23	0·22	0·19	0·19	0·12
Cr_2O_3	0·05	0·01	0·00	0·13	0·03	0·05	0·06	0·05	0·05	0·04	0·07
Ba	n.a.	n.a.	n.a.	n.a.	n.a.	n.a.	16·55	18·08	18·07	14·81	8·80
Nb	n.a.	n.a.	n.a.	n.a.	n.a.	n.a.	4·34	5·14	5·02	4·15	1·21
La	n.a.	n.a.	n.a.	n.a.	n.a.	n.a.	6·33	6·55	7·52	6·19	2·51
Ce	n.a.	n.a.	n.a.	n.a.	n.a.	n.a.	17·23	20·06	22·12	18·43	8·89
Pr	n.a.	n.a.	n.a.	n.a.	n.a.	n.a.	2·67	2·58	3·34	2·61	1·43
Sr	n.a.	n.a.	n.a.	n.a.	n.a.	n.a.	195	225	228	225	107
Nd	n.a.	n.a.	n.a.	n.a.	n.a.	n.a.	11·96	13·14	16·14	13·11	9·00
Hf	n.a.	n.a.	n.a.	n.a.	n.a.	n.a.	3·12	3·07	3·07	2·69	2·49
Zr	n.a.	n.a.	n.a.	n.a.	n.a.	n.a.	103	141	156	129	78
Sm	n.a.	n.a.	n.a.	n.a.	n.a.	n.a.	3·51	4·65	4·71	3·61	3·03
Eu	n.a.	n.a.	n.a.	n.a.	n.a.	n.a.	0·89	1·11	1·13	1·00	1·02
Gd	n.a.	n.a.	n.a.	n.a.	n.a.	n.a.	4·20	6·49	5·32	4·09	3·88
Tb	n.a.	n.a.	n.a.	n.a.	n.a.	n.a.	0·74	1·00	0·96	0·76	0·80
Dy	n.a.	n.a.	n.a.	n.a.	n.a.	n.a.	4·61	5·33	6·02	5·46	4·20
Y	n.a.	n.a.	n.a.	n.a.	n.a.	n.a.	34·25	36·40	40·50	35·18	29·33
Ho	n.a.	n.a.	n.a.	n.a.	n.a.	n.a.	1·04	1·14	1·28	1·07	0·86
Er	n.a.	n.a.	n.a.	n.a.	n.a.	n.a.	3·01	3·48	3·93	3·54	2·78
Yb	n.a.	n.a.	n.a.	n.a.	n.a.	n.a.	3·06	3·27	3·54	3·21	2·59

(continued)

Downloaded from petrology.oxfordjournals.org by guest on May 18, 2011

Table 5: Continued

Sample:	DR51	DR51	DR61	DR61	DR61	DR61	DR61	DR61	DR61	DR61	DR75
MI:	EE	EG	AC-107	AE-109	AL-114	AM-115	AP-118	AQ-119	150	152	BV-89
Host:	Pl 1	Pl 1	Pl 4	Pl 4	Pl 4	Pl 4	Pl 4	Pl 4	Ol 1	Ol 2	Pl 3
SiO_2	50·72	50·25	50·99	50·92	49·96	49·87	49·90	49·69	50·25	50·01	50·34
TiO_2	1·12	1·20	1·08	1·14	1·61	1·68	1·66	1·62	2·03	1·96	0·72
Al_2O_3	16·35	16·39	16·56	16·64	16·59	16·39	16·37	16·72	15·12	15·17	16·82
FeO*	8·98	9·10	9·08	9·07	9·26	9·41	9·43	9·27	10·91	11·18	7·47
MnO	0·16	0·17	0·17	0·17	0·15	0·19	0·17	0·17	0·22	0·20	0·15
MgO	7·97	8·17	7·62	7·55	7·64	7·64	7·62	7·56	6·80	6·78	9·08
CaO	11·34	11·48	11·15	10·95	11·33	11·38	11·41	11·36	10·77	10·93	13·32
Na_2O	3·12	2·99	3·02	3·26	3·09	3·08	3·05	3·24	3·37	3·23	2·00
K_2O	0·09	0·10	0·16	0·15	0·14	0·15	0·15	0·17	0·19	0·18	0·02
P_2O_5	0·11	0·09	0·11	0·10	0·19	0·17	0·20	0·18	0·30	0·30	0·06
Cr_2O_3	0·06	0·07	0·06	0·05	0·04	0·04	0·06	0·03	0·05	0·07	0·04
Ba	8·99	9·46	12·95	11·47	17·37	n.a.	n.a.	n.a.	17·04	n.a.	n.a.
Nb	1·81	2·09	2·21	2·12	3·83	n.a.	n.a.	n.a.	3·83	n.a.	n.a.
La	2·96	2·79	3·57	3·37	5·73	n.a.	n.a.	n.a.	6·01	n.a.	n.a.
Ce	8·57	9·47	10·83	10·05	18·00	n.a.	n.a.	n.a.	18·40	n.a.	n.a.
Pr	1·49	1·56	1·80	1·51	2·97	n.a.	n.a.	n.a.	3·07	n.a.	n.a.
Sr	103	104	144	135	141	n.a.	n.a.	n.a.	144	n.a.	n.a.
Nd	8·32	9·68	8·87	9·01	15·39	n.a.	n.a.	n.a.	16·31	n.a.	n.a.
Hf	2·02	1·83	2·41	2·00	3·64	n.a.	n.a.	n.a.	3·26	n.a.	n.a.
Zr	82	76	80	78	147	n.a.	n.a.	n.a.	151	n.a.	n.a.
Sm	2·79	3·31	3·40	2·99	5·64	n.a.	n.a.	n.a.	5·44	n.a.	n.a.
Eu	0·85	0·83	1·03	0·88	1·15	n.a.	n.a.	n.a.	0·98	n.a.	n.a.
Gd	3·26	3·20	3·24	3·33	5·75	n.a.	n.a.	n.a.	5·33	n.a.	n.a.
Tb	0·59	0·66	0·61	0·63	0·96	n.a.	n.a.	n.a.	1·02	n.a.	n.a.
Dy	3·73	4·21	4·24	4·23	6·93	n.a.	n.a.	n.a.	7·19	n.a.	n.a.
Y	27·53	29·12	27·98	27·77	44·45	n.a.	n.a.	n.a.	45·77	n.a.	n.a.
Ho	0·82	0·81	0·87	0·76	1·37	n.a.	n.a.	n.a.	1·63	n.a.	n.a.
Er	2·52	2·83	2·59	2·71	4·25	n.a.	n.a.	n.a.	4·59	n.a.	n.a.
Yb	2·73	2·42	2·30	2·56	4·04	n.a.	n.a.	n.a.	4·11	n.a.	n.a.

Downloaded from petrology.oxfordjournals.org by guest on May 18, 2011

Table 5: Continued

Sample:	DR75	DR75	DR75	DR75	DR75	DR75
MI:	CE-98	CJ-103	CK-104	HH-100	HI-101	HE-97
Host:	Pl 3	Pl 3	Pl 3	Ol 2	Ol 2	Ol 1
SiO_2	50·19	49·91	49·94	50·03	49·91	50·29
TiO_2	0·77	0·98	0·99	1·65	1·62	1·64
Al_2O_3	16·85	16·54	16·70	14·29	14·26	14·93
FeO*	7·44	7·58	7·56	12·29	12·39	11·09
MnO	0·14	0·14	0·13	0·22	0·23	0·20
MgO	8·92	9·10	9·05	7·21	7·13	7·68
CaO	13·54	13·50	13·36	11·38	11·59	11·05
Na_2O	2·04	2·10	2·11	2·71	2·61	2·87
K_2O	0·03	0·02	0·03	0·07	0·07	0·07
P_2O_5	0·06	0·08	0·08	0·13	0·16	0·16
Cr_2O_3	0·03	0·08	0·05	0·03	0·04	0·03
Ba	n.a.	n.a.	n.a.	n.a.	n.a.	n.a.
Nb	n.a.	n.a.	n.a.	n.a.	n.a.	n.a.
La	n.a.	n.a.	n.a.	n.a.	n.a.	n.a.
Ce	n.a.	n.a.	n.a.	n.a.	n.a.	n.a.
Pr	n.a.	n.a.	n.a.	n.a.	n.a.	n.a.
Sr	n.a.	n.a.	n.a.	n.a.	n.a.	n.a.
Nd	n.a.	n.a.	n.a.	n.a.	n.a.	n.a.
Hf	n.a.	n.a.	n.a.	n.a.	n.a.	n.a.
Zr	n.a.	n.a.	n.a.	n.a.	n.a.	n.a.
Sm	n.a.	n.a.	n.a.	n.a.	n.a.	n.a.
Eu	n.a.	n.a.	n.a.	n.a.	n.a.	n.a.
Gd	n.a.	n.a.	n.a.	n.a.	n.a.	n.a.
Tb	n.a.	n.a.	n.a.	n.a.	n.a.	n.a.
Dy	n.a.	n.a.	n.a.	n.a.	n.a.	n.a.
Y	n.a.	n.a.	n.a.	n.a.	n.a.	n.a.
Ho	n.a.	n.a.	n.a.	n.a.	n.a.	n.a.
Er	n.a.	n.a.	n.a.	n.a.	n.a.	n.a.
Yb	n.a.	n.a.	n.a.	n.a.	n.a.	n.a.

The compositions are all corrected to a 100% total. MI, melt inclusion; n.a., not analysed.

Data Appendix 1, available for downloading at http://www.petrology.oxfordjournals.org). Michael *et al.* (2002) suggested that the HFSE depletion in plagioclase-hosted melt inclusions is caused by dissolution of plagioclase to form a melt that is depleted in such elements. Diffusion through the walls of the plagioclase host then moves the inclusion compositions towards that of the external melt, with fast diffusing elements equilibrating before the slower diffusing HFSE. In contrast, Nielsen & Sours-Page (2000) proposed a hydrothermally altered, depleted peridotite source for the melt trapped in these depleted melt inclusions. The discarded plagioclase-hosted melt inclusions in this study, which plotted outside the MORB and SWIR glass field and are characterized by very low Fe–Ti and HREE but high Na, probably represent melts that were formed by the mixture of the originally entrapped melt and dissolved host plagioclase.

Indicators of melt fraction, depth of melting and source composition

To account for the effects of fractional crystallization on both melt inclusions and matrix glass, the major element data are normalized to 8 wt % MgO [following the method of Klein & Langmuir (1987)]. The Na_8 and K_8 values are used to estimate the degree of melting generated

Downloaded from petrology.oxfordjournals.org by guest on May 18, 2011

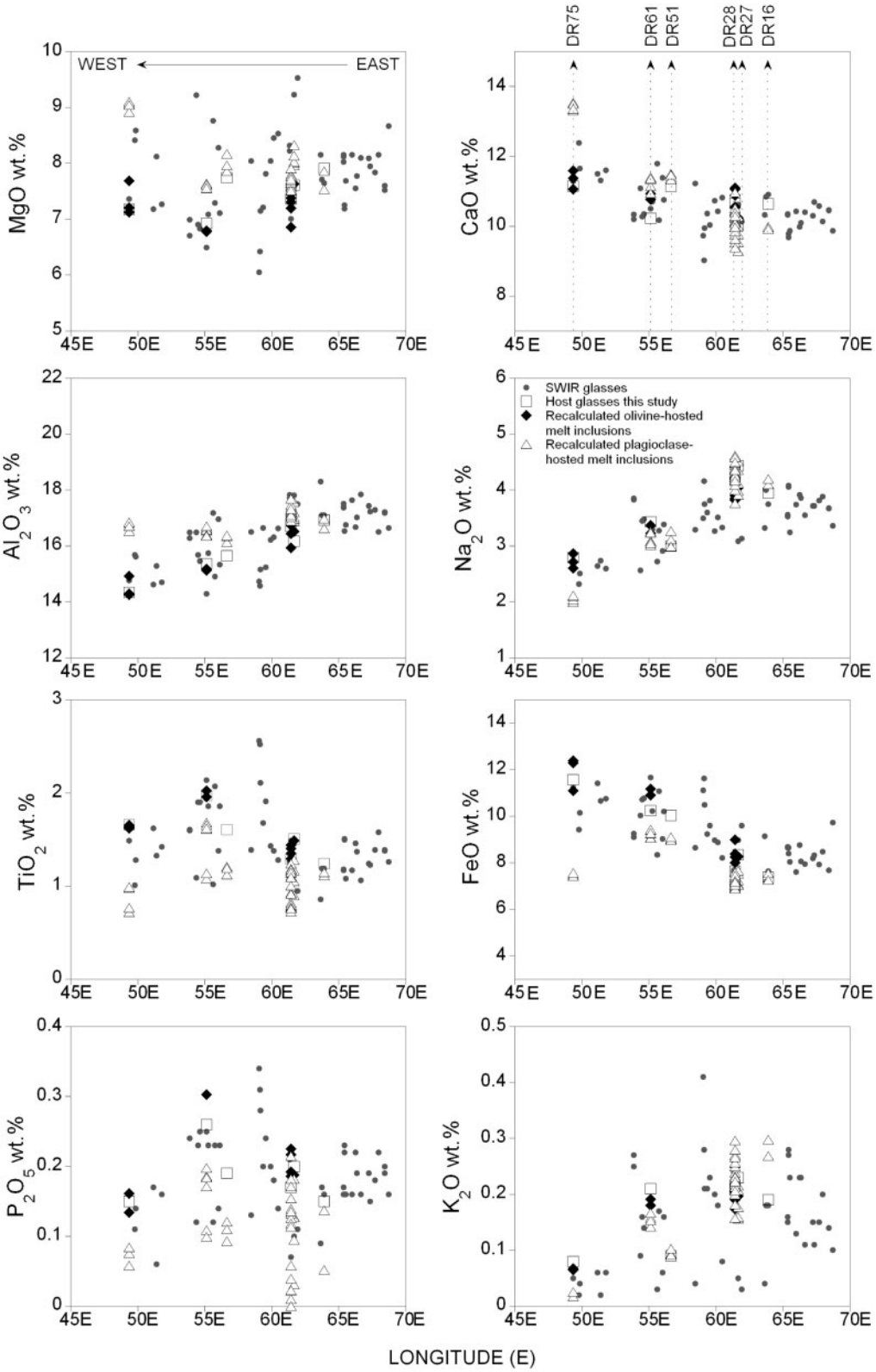

Fig. 5. Major element diagrams vs longitude (°E) of recalculated olivine-hosted melt inclusion compositions (◆), recalculated plagioclase-hosted melt inclusion compositions (△), host glasses (□) and Southwest Indian Ridge glass data (Meyzen *et al.*, 2003) (●).

Downloaded from petrology.oxfordjournals.org by guest on May 18, 2011

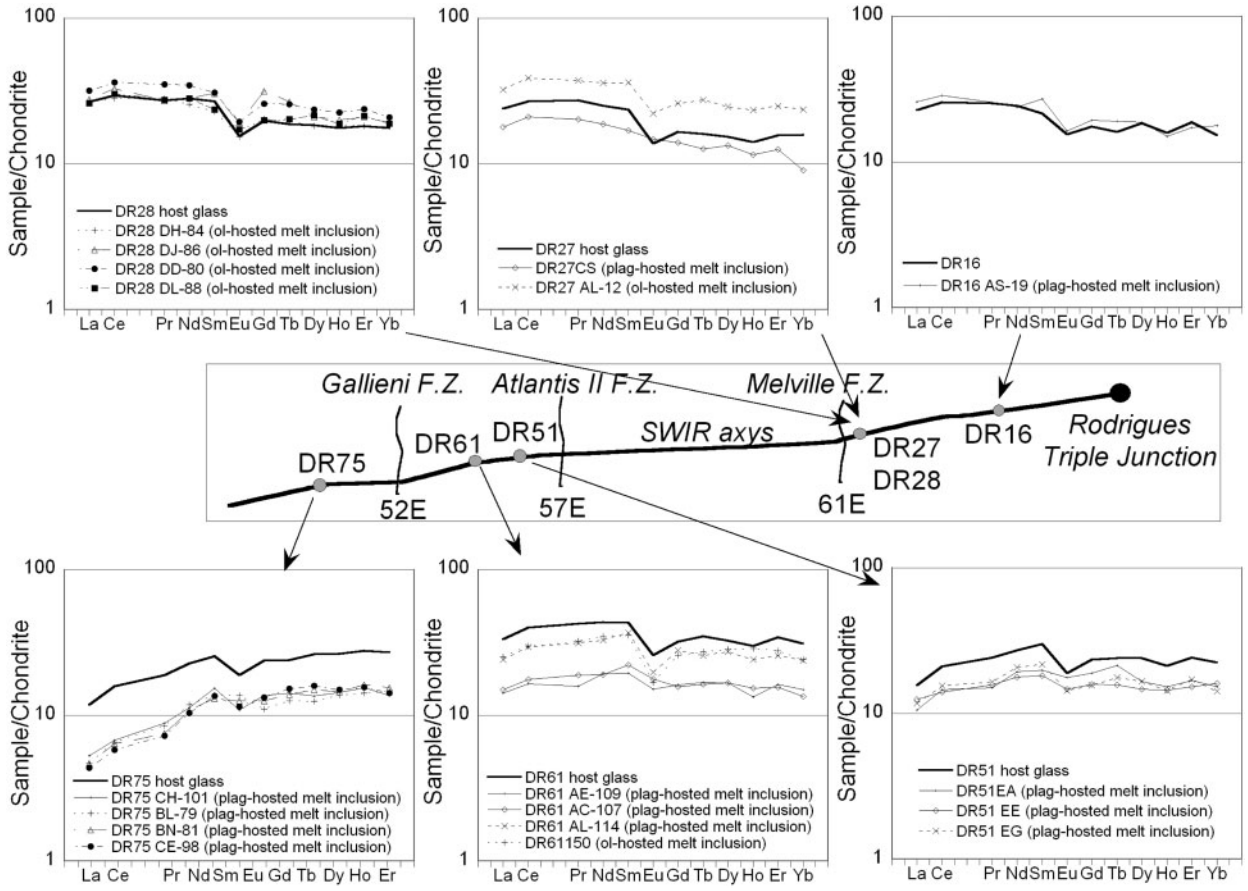

Fig. 6. Chondrite-normalized (Sun & McDonough, 1989) REE patterns of host glasses and melt inclusions for different locations along the SWIR.

at mid-ocean ridges (Klein & Langmuir, 1987; Langmuir *et al.*, 1992); both Na and K behave incompatibly during partial melting, and are therefore preferentially partitioned into the melt at low degrees of melting. Other incompatible trace elements, including the REE, which are partitioned into the melt, also act as indicators of the degree of partial melting [e.g. $(La/Sm)_n$]. Parameters such as Fe_8 are used as indicators of the depth of melting (Klein & Langmuir, 1987; Langmuir *et al.*, 1992).

The host glasses and melt inclusions show a decrease in Na_8 and K_8 values and a corresponding increase in Fe_8 values, from 64°E to 49°E (Fig. 7). Klein & Langmuir (1987) suggested that a progressive decrease in Na_8 indicates an increase in degree of partial melting of a spinel lherzolite mantle source, whereas an increase in Fe_8 indicates an increase in average depth of melting. Thus, the decrease in Na_8 for both the host glasses and melt inclusions towards 49°E suggests an increase in the degree of partial melting towards the SW part of the SWIR (64°E–49°E). Similarly, the increasing Fe_8 shown by the host glasses and the melt inclusions towards 49°E suggests greater average depth of melting to the SW of the SWIR and, hence, a higher mantle temperature. This is consistent with a NE to SW regional increase in axial depth along the SWIR (Cannat *et al.*, 1999) and an increase in the abundance of volcanoes within the area (Mendel *et al.*, 1997), and it is evidence for the increasing temperature of the underlying mantle (Sauter *et al.*, 2001).

East of the Melville FZ, the olivine- and plagioclase-hosted melt inclusions have low Fe_8 (Fig. 7); in contrast, their Na_8 values are much higher, and show a large variation (Fig. 7). The low Fe_8 values suggest that these melt inclusions are segregated at relatively shallow depths in the melting column, whereas the high, but diverse, Na_8 values indicate melt segregation at low degrees of melting. West of the Melville FZ, the melt inclusions show a progressive increase (with increasing distance to the west from the Melville FZ) in Fe_8 variability, with those hosted within olivine having progressively higher Fe_8 values compared with those hosted in plagioclase. This suggests that the olivine-hosted melt inclusions were segregated from the mantle at a greater average depth than the

Downloaded from petrology.oxfordjournals.org by guest on May 18, 2011

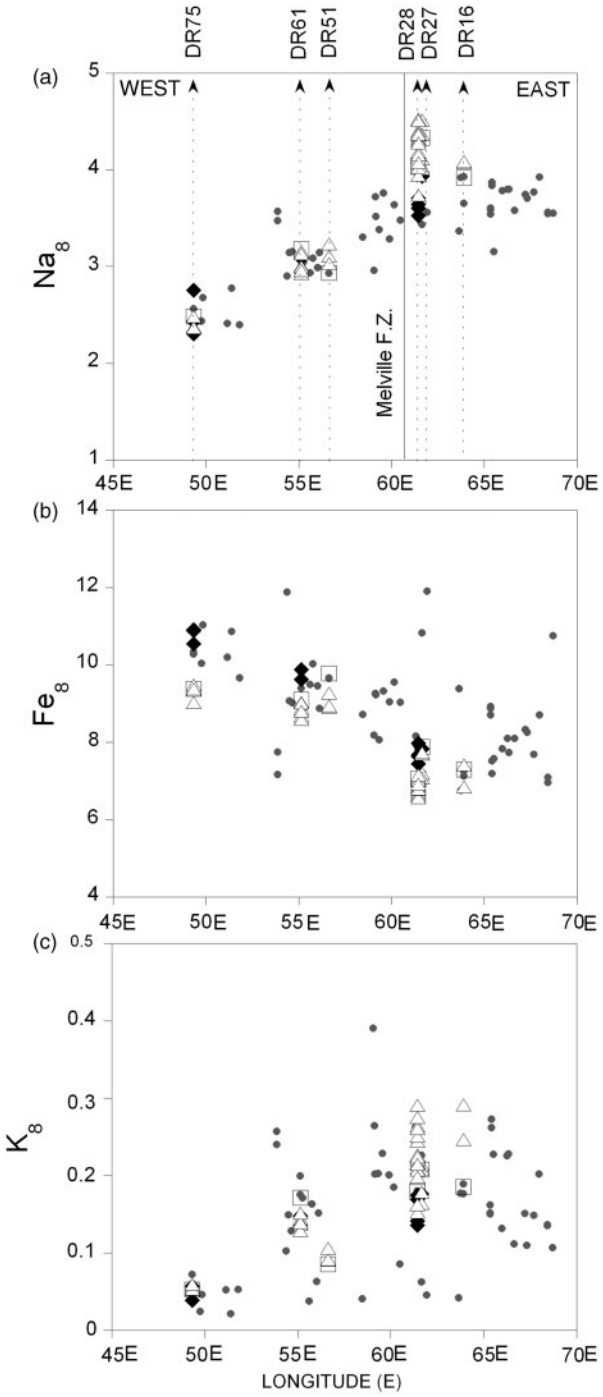

Fig. 7. Na_8 (a), Fe_8 (b) and K_8 (c) vs longitude. Symbols as in Fig. 5.

plagioclase-hosted melt inclusions. This is consistent with the depleted compositions of the plagioclase-hosted melt inclusions (e.g. from the samples at 57°E and 49°E), and their shallow depth of melting, compared with the olivine-hosted melt inclusions. The Fe_8 values and depleted compositions indicate that these shallow melts represent some of the last melt fractions produced from the mantle column.

The basaltic glasses from the SWIR between 64°E and 49°E have previously been reported to form two distinct compositional groups, distinguished by their Na_8, Fe_8 and trace elements ratios [such as $(Sm/Yb)_n$; see Meyzen *et al.*, 2003]. These two compositional domains, separated by the Melville FZ (Mendel *et al.*, 1997; Meyzen *et al.*, 2003) have been attributed to compositional differences in the mantle source beneath the NE end of the SWIR. It has been suggested that the mantle source to the east of the Melville FZ is depleted in clinopyroxene as a consequence of partial melting followed by refertilization of the depleted source, generating the enrichment in LREE and Na observed in the lavas from this region. To the west of the Melville FZ, the composition of the glasses is consistent with a progressive increase, from NE to SW, in the degree of partial melting of a refertilized lherzolite source (Meyzen *et al.*, 2003). The Na_8 and Fe_8 values of the melt inclusions also separate into the two compositional groups defined by the SWIR glasses (Fig. 8), with higher Na_8 values to the east of the Melville fracture zone, and higher Fe_8 to the west. The chondrite-normalized REE patterns of melt inclusions (Fig. 8) from samples between 64°E and 61°E (east of the Melville FZ) show LREE enrichment but slight depletion in HREE, suggesting that the melt inclusions were derived from a source previously melted to relatively high degrees to the point where the source became depleted in clinopyroxene and was subsequently refertilized, becoming enriched in LREE. The higher Na_8 of these melt inclusions, which agrees with the glass data, also suggests that the source has been refertilized as indicated by Meyzen *et al.* (2003). None of the SWIR melt inclusion REE patterns appear to be as depleted as those of the Mid-Atlantic Ridge ultra-depleted olivine-hosted melt inclusions studied by Sobolev & Shimizu (1993) (Fig. 8), suggesting that complete exhaustion of clinopyroxene in the source did not occur.

Melt inclusions from samples at 57°E (DR51) and 49°E (DR75), west of the Melville FZ, are depleted in LREE with respect to the HREE (Figs 6 and 8). The more strongly depleted REE patterns of the melt inclusions in sample DR75 compared with sample DR51 suggest an increase in the degree of partial melting westwards along the SWIR. However, melt inclusions from sample DR61 located at 55°E, west of the Melville FZ, also show enrichment in LREE similar to the samples to the east of the Melville FZ, but have flat patterns for the HREE, suggesting that the melt source is not depleted in clinopyroxene (Fig. 6). The similarities in composition of the melt inclusions from sample DR61 at 55°E to the samples east of Melville FZ suggest that these melts are also derived from a source that has been enriched in LREE, probably by the same metasomatic fluids that affected the source

Downloaded from petrology.oxfordjournals.org by guest on May 18, 2011

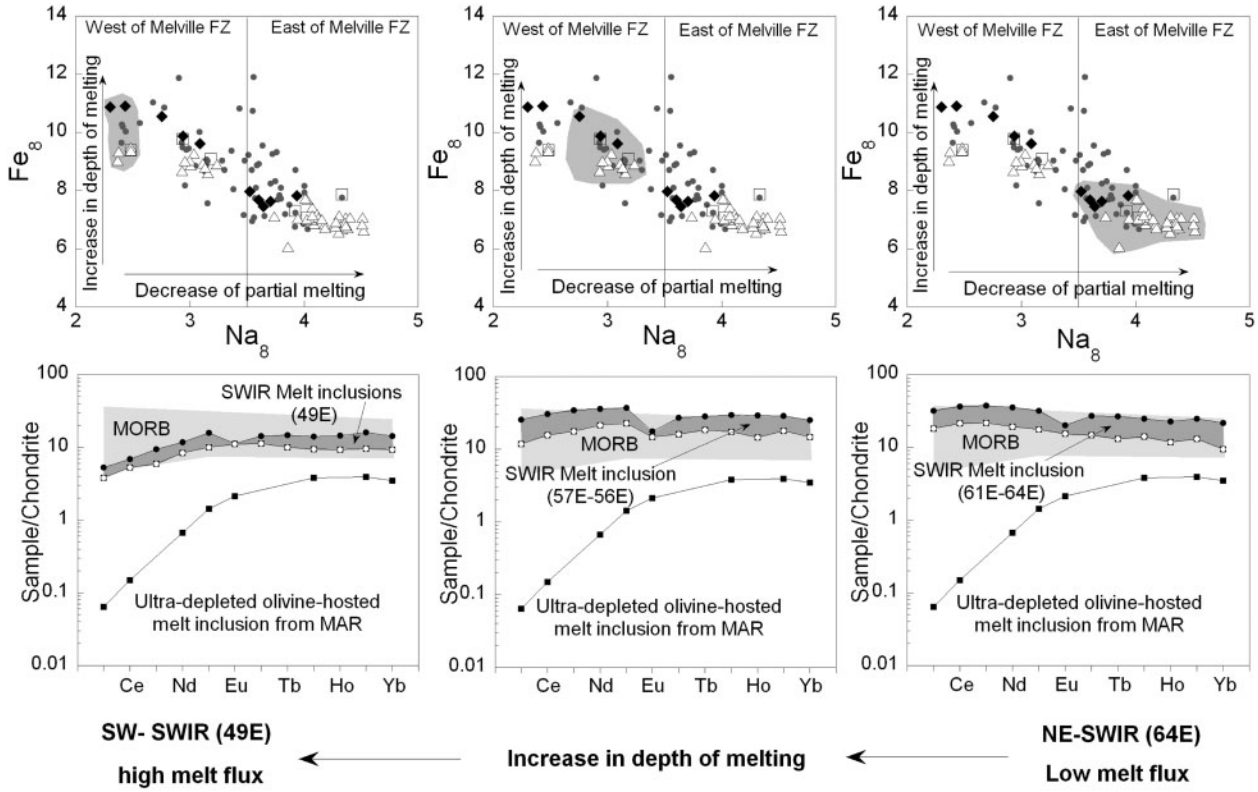

Fig. 8. Longitudinal Fe_8 vs Na_8 variation of recalculated melt inclusion compositions and chondrite-normalized REE patterns of melt inclusions compared with the MORB field and ultra-depleted olivine-hosted melt inclusions from the Mid-Atlantic Ridge (MAR) (Sobolev & Shimizu, 1993). Symbols as in Fig. 5.

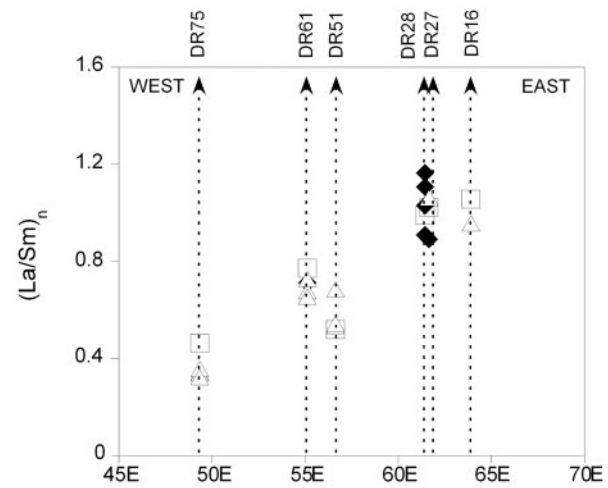

Fig. 9. Chondrite-normalized $(La/Sm)_n$ (Sun & McDonough 1989) vs longitude (°E). Symbols as in Fig. 5.

region to the east of Melville FZ. This interpretation is supported by variations in trace element ratios such as $(La/Sm)_n$, which are also indicators of variations in the degree of mantle partial melting and/or source composition.

From the NE to the SW part of the SWIR, the host glasses and melt inclusions show a general decrease in $(La/Sm)_n$. This is consistent with an increase in the degree of partial melting towards the SW (Fig. 9). However, melt inclusions and matrix glass from sample DR61 have higher $(La/Sm)_n$ values compared with samples DR51 and DR75. This indicates, despite the general decrease in trace element ratios, that there is local magma enrichment.

The model proposed in this study to explain the compositional differences observed in the melt inclusions and host glasses is summarized in Fig. 10. The degree of partial melting, between 70°E and 49°E along the SWIR, increases from NE to SW. Melts east of the Melville FZ are generated at shallow depths in the mantle melting column. Melts west of the Melville FZ, initially generated deep in the mantle melting column, become trapped within olivine when they reach the magma chamber. As mantle melting continues, melts from the shallower, depleted parts of the mantle melting column are removed and arrive in the magma chamber. By this time plagioclase is crystallizing in the magma chamber and these shallow depleted melts become trapped. The compositional diversity observed in melts from the east of the Melville FZ also suggests episodic magma supply and low degrees of mantle melting.

Downloaded from petrology.oxfordjournals.org by guest on May 18, 2011

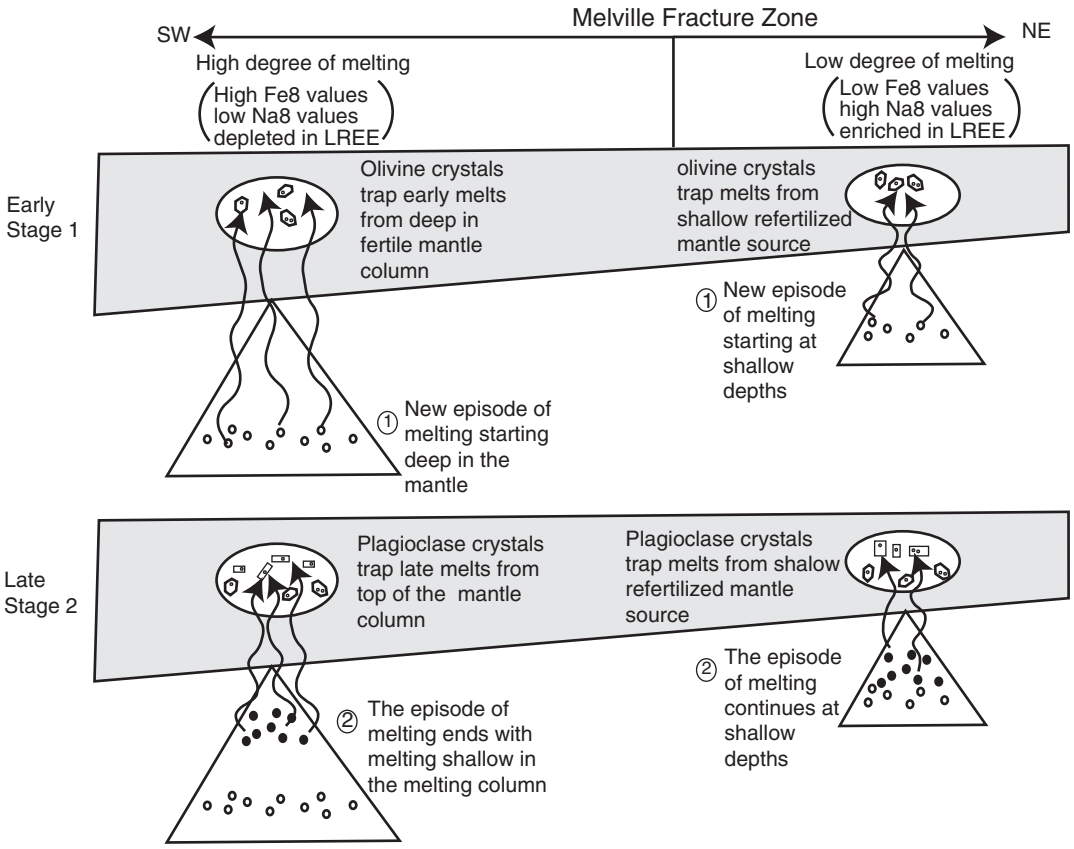

Fig. 10. Schematic illustration of the variation in depth of melt segregation in the mantle melting column and melt inclusion entrapment along the SWIR between 70°E and 49°E.

CONCLUSIONS

Olivine- and plagioclase-hosted melt inclusions from the 64°E–49°E region of the Southwest Indian Ridge show an increase in the degree of fractional crystallization towards the SW. Melt inclusions from the NE end of the ridge (64°E–61°E) exhibit more compositional diversity compared with those from the SW (55°E–49°E). Like their host glasses, the melt inclusions also have increasing Na_8 and decreasing Fe_8 values to the NE. This suggests that the ridge in this region is supplied by a range of different melt batches generated by low degrees of melting at shallow levels within a spinel lherzolite source. However, towards the SW, where the ridge is supplied by higher degree melts and the melt compositions become progressively more depleted in LREE, local enrichments of the melt source also occur. This is shown by melt inclusions from sample DR61 at 57°E, in which LREE-enriched compositions are superimposed on low Na_8 and high Fe_8 LREE-depleted compositions. The depleted composition of plagioclase-hosted melt inclusions from sample DR75 at 49°E indicates that these melts are the last melts segregated from a depleted source at very shallow levels.

The olivine-hosted melt inclusions typically show similar compositions to the host glasses but, compared with plagioclase-hosted melt inclusions, they show progressively higher Fe_8 values towards the SW end of the ridge, with the greatest variation at 49°E. This suggests that the olivine-hosted melt inclusions represent melt batches that were formed at a greater depth than the plagioclase-hosted ones.

ACKNOWLEDGEMENTS

We wish to thank Leonid Danyushevsky, Peter Michael and Jon P. Davidson for their helpful reviews, and editor M. Wilson for the helpful comments and suggestions. This paper is part of L. Font's Ph.D. thesis supported by a Ph.D. scholarship from the University of Southampton and the School of Ocean and Earth Sciences. The ion microprobe analyses were supported by the NERC grant IMP181/1001.

SUPPLEMENTARY DATA

Supplementary data for this paper are available at *Journal of Petrology* online.

Downloaded from petrology.oxfordjournals.org by guest on May 18, 2011

REFERENCES

Bown, J. W. & White, R. S. (1994). Variation with spreading rate of oceanic crustal thickness and geochemistry. *Earth and Planetary Science Letters* **121**, 435–449.

Cannat, M., Rommevaux-Jestin, C., Suter, D., Deplus, C. & Mendel, V. (1999). Formation of axial relief at the very slow spreading Southwest Indian Ridge. *Journal of Geophysical Research* **104**, 22825–22843.

Chu, D. & Gordon, R. G. (1999). Evidence for motion between Nubia and Somalia along the Southwest Indian Ridge. *Nature* **398**, 64–67.

Danyushevsky, L. (2001). The effects of small amounts of H_2O on crystallisation of mid-ocean ridge and back arc basin magmas. *Journal of Volcanology and Geothermal Research* **110**, 265–280.

Danyushevsky, L., McNeill, A. W. & Sobolev, A. V. (2002). Experimental and petrological studies of melt inclusions in phenocrysts from mantle-derived magmas: an overview of techniques, advantages and complications. *Chemical Geology* **183**, 5–24.

Danyushevsky, L., Della-Pasqua, F. N. & Sokolov, S. (2000). Re-equilibration of melt inclusions trapped by magnesian olivine phenocrysts from subduction-related magmas: petrological implications. *Contributions to Mineralogy and Petrology* **138**, 68–83.

de Ribet, B. & Patriat, P. (1988). The axial region of the Southwest Indian ridge between 53°E and 59°E: evolution during the last 10 Ma. *Marine Geophysical Research* **10**, 139–156.

Dick, H. J. B., Lin, J. & Schouten, H. (2003). An ultraslow-spreading class of ocean ridge. *Nature* **426**, 405–412.

Fowler, C. M. R. (1976). Crustal structure of the mid-Atlantic ridge crest at 37°E. *Geophysical Journal of the Royal Astronomical Society* **47**, 459–491.

Fowler, C. M. R. (1978). The mid-Atlantic ridge: structure at 45°E. *Geophysical Journal of the Royal Astronomical Society* **54**, 167–183.

Fery, F. A., Dickey, J. S. Jr., Thompson, G., Bryan, W. B. & Davis, H. L. (1980). Evidence for heterogeneous primary MORB and mantle sources, NW Indian Ocean. *Contributions to Mineralogy and Petrology* **74**, 387–402.

Gaetani, G. A. & Watson, E. B. (2002). Modeling the major-element evolution of olivine-hosted melt inclusions. *Chemical Geology* **183**, 25–41.

Irving, A. J. & Frey, F. A. (1984). Trace element abundances in megacrysts and their host basalts: constraints on partition coefficients and megacrysts genesis. *Geochimica et Cosmochimica Acta* **48**, 1201–1221.

Klein, E. M. & Langmuir, C. H. (1987). Global correlations of ocean ridge basalt chemistry with axial depth and crustal thickness. *Journal of Geophysical Research* **92**, 8089–8115.

Kohut, E. & Nielsen, R. L. (2004). Melt inclusion formation mechanisms and compositional effects in high-An feldspar and high-Fo olivine in anhydrous mafic silicate liquids. *Contributions to Mineralogy and Petrology* **147**, 684–704.

Langmuir, C. H., Klein, E. M. & Plank, T. (1992). Petrological systematics of mid-ocean ridge basalts: constraints on melt generation beneath ocean ridges. In: Phipps Morgan, J., Blackman, D. K. & Sinton, J. M. (eds) *Mantle Flow and Melt Generation at Mid-ocean Ridges. Geophysical Monographs, American Geophysical Union* **71**, 281–310.

Le Roex, A. P., Dick, H. J. B., Erlank, A. J., Reid, A. M., Frey, F. A. & Hart, S. R. (1983). Geochemistry, mineralogy and petrogenesis of lavas erupted along the Southwest Indian Ridge, between the Bouvet Triple Junction and 11 degrees East. *Journal of Petrology* **24**, 267–318.

Mahoney, J. J., Natland, J. H., White, W. M., Poreda, R. & Bloomer, S. H. (1989). Isotopic and geochemical provinces of the Indian ocean spreading centres. *Journal of Geophysical Research* **94**, 4033–4052.

McKenzie, D. (1985). The extraction of magma from the crust and mantle. *Earth and Planetary Science Letters* **74**, 81–91.

Mendel, V., Sauter, D., Parson, L. & Vanney, J. R. (1997). Segmentation and morphotectonic variations along a super slow-spreading centre: the Southwest Indian Ridge (57°E–70°E). *Marine Geophysical Researches* **19**, 505–533.

Mével, C., Toplis, M. J., Humler, E., Meyzen, C. & Ludden, J. (2002). Major and rare earth element zoning of plagioclase in basalts from the Southwest Indian Ridge (69–49°E). In: Adamczewska, A. & Kaczmarz, M. (eds.) *South West Indian Ridge—InterRidge Workshop Abstracts Volume, InterRidge, Tokyo, pp.52.*

Meyzen, C., Toplis, M., Humler, E., Ludden, J. & Mével, C. (2003). A discontinuity in mantle composition beneath the Southwest Indian ridge. *Nature* **421**, 731–733.

Michael, P., McDonough, W. F., Nielsen, R. L. & Cornell, W. C. (2002). Depleted melt inclusions in MORB plagioclase: message from the mantle or mirages from the magma chamber? *Chemical Geology* **183**, 43–61.

Minshull, T. & White, R. S. (1996). Thin crust on the flanks of the slow-spreading Southwest Indian Ridge. *Geophysical Journal International* **125**, 139–148.

Muller, M. R., Minshull, T. A. & White, R. S. (1999). Segmentation and melt supply of the Southwest Indian Ridge. *Geology* **27**, 867–870.

Muller, M. R., Minshull, T. A. & White, R. S. (2000). Crustal structure of the Southwest Indian Ridge at the Atlantis II Fracture Zone. *Journal of Geophysical Research (Solid Earth)* **105**(B11), 25809–25828.

Murton, B. J. & Parson, L. (1993). Segmentation, volcanism and deformation of oblique spreading centers: a quantitative study of the Reykjianes ridge. *Tectonophysics* **222**, 237–257.

Natland, J. (1991). Indian ocean crust. In: Floyd, P. A. (ed.) *Oceanic Basalts*. New York: Blackie, pp. 299–352.

Nielsen, R. L. & Sours-Page, R. E. (2000). Role of a Cl-bearing flux in the origin of depleted ocean floor magmas. *Geochemistry, Geophysics, Geosystems* paper number 1999GC000017.

Price, R. C., Kennedy, A. K., Riggs-Sneeringer, M. & Frey, F. A. (1986). Geochemistry of basalts from the Indian Ocean triple junction: implications for the generation and evolution of Indian Ocean Ridge basalts. *Earth and Planetary Science Letters* **78**, 379–396.

Purdy, G. M. & Detrick, R. S. (1986). Crustal structure of the Mid-Atlantic Ridge at 23°N from seismic refraction studies. *Journal of Geophysical Research—Solid Earth and Planets* **91**, 3739–3762.

Reid, I. & Jackson, H. R. (1981). Oceanic spreading rate and crustal thickness. *Marine Geophysical Researches* **5**, 165–172.

Robinson, C. (1998). Mantle melting and crustal generation at the very slow spreading Southwest Indian Ridge. Ph.D. thesis, University of Cambridge.

Robinson, C., Bickle, M. J., Minshull, T. A., White, R. S. & Nichols, A. R. L. (2001). Low degree melting under the Southwest Indian Ridge: the roles of mantle temperature, conductive cooling and wet melting. *Earth and Planetary Science Letters* **188**, 383–398.

Roedder, E. (1984). *Fluid Inclusions. Mineralogical Society of America, Reviews in Mineralogy* **12**, 643 pp.

Sauter, D., Patriat, P., Rommevaux-Jestin, C., Cannat, M., Briais, A. & Gallieni Shipboard Scientific Party, (2001). The Southwest Indian Ridge between 49°15'E and 57°E: focused accretion and magma redistribution. *Earth and Planetary Science Letters* **192**, 303–317.

Scalter, J. G., Fisher, R. L., Patriat, P., Tapscott, C. & Parsons, B. (1981). Eocene to recent development of the Southwest Indian Ridge, a consequence of the evolution of the Indian Ocean triple junction. *Geophysical Journal of the Royal Astronomical Society* **64**, 587–604.

Downloaded from petrology.oxfordjournals.org by guest on May 18, 2011

Sinton, J. M. & Detrick, R. S. (1993). Mid-Ocean Ridge magma chambers. *Journal of Geophysical Research* **97**, 197–216.

Sobolev, A. V. & Shimizu, N. (1993). Ultra-depleted primary melt included in an olivine from the Mid-Atlantic Ridge. *Nature* **363**, 151–153.

Sobolev, A. V. & Shimizu, N. (1994). The origin of typical NMORB: the evidence from a melt inclusions study. *Mineralogical Magazine* **58A**, 862–863.

Sours-Page, R., Johnson, K. T. M, Nielsen, R. L. & Karsten, J. L. (1999). Local and regional variation of MORB parent magmas: evidence from melt inclusions from the Endeavour Segment of Juan de Fuca Ridge. *Contributions to Mineralogy and Petrology* **134**, 342–363.

Sours-Page, R., Nielsen, R. L. & Batiza, R. (2002). Melt inclusions as indicators of parental magma diversity on the northern East Pacific Rise. *Chemical Geology* **183**, 237–261.

Sun, S. S. & McDonough, W. F. (1989). Chemical and isotopic systematics of oceanic basalts: implications for mantle composition and processes. In: Saunders, A. D. & Norry, M. J. (eds) *Magmatism in the Ocean Basins. Geological Society, London, Special Publication* **42**, 313–345.

Downloaded from petrology.oxfordjournals.org by guest on May 18, 2011